AN ABSTRACT OF THE THESIS OF

Pukha Lenee-Bluhm for the Master of Science in Mechanical Engineering presented on May 28, 2010.

Title: The Wave Energy Resource of the US Pacific Northwest.

Abstract approved:

Robert K. Paasch

The substantial wave energy resource of the US Pacific Northwest (i.e. off the coasts of Washington, Oregon and N. California) is assessed and characterized. Archived spectral records from ten wave measurement buoys, operated and maintained by the National Data Buoy Center and the Coastal Data Information Program, form the basis of this investigation. Because an ocean wave energy converter must reliably convert, and survive, the energetic resource, a comprehensive characterization of the expected range of sea states is essential. Six quantities were calculated to characterize each hourly sea state: omnidirectional wave power, significant wave height, energy period, spectral width, direction of maximum directionally resolved wave power and directionality coefficient. The temporal variability of these characteristic quantities is depicted at different scales, from hourly to interannual. Cumulative distributions of both occurrence and contribution to total energy are presented, over each of the six quantities characterizing the resource. It is clear that the sea states occurring most often are not necessarily those that contribute most to the total incident wave energy. The sea states with the greatest contribution to energy have significant wave heights between 2 and 5 m and energy periods between 8 and 12 s. Sea states with the greatest significant wave heights (e.g. > 7 m) contribute little to the annual energy, but are critical to consideration of reliability and survivability. To characterize the likelihood of successfully performing a given

operation (e.g. deployment, maintenance), seasonal expectations of weather windows are depicted for two locations. Finally, a limited number of spectra are proposed to represent the conditions at a location 9 km offshore, in 40 m of water.

The Wave Energy Resource of the US Pacific Northwest

by

Pukha Lenee-Bluhm

A THESIS

submitted to

Oregon State University

in partial fulfillment of
the requirements for the
degree of

Master of Science

Presented May 28, 2010
Commencement June 2010

Master of Science thesis of Pukha Lenee-Bluhm presented on May 28, 2010.

APPROVED:

Major Professor, representing Mechanical Engineering

Head of the School of Mechanical, Industrial and Manufacturing Engineering

Dean of the Graduate School

I understand that my thesis will become part of the permanent collection of Oregon State University libraries. My signature below authorizes release of my thesis to any reader upon request.

Pukha Lenee-Bluhm, Author

ACKNOWLEDGEMENTS

Rise up nimbly and go on your strange journey
to the ocean of meanings.

The stream knows it can't stay on the mountain.
Leave and don't look away from the sun as you go,
in whose light you're sometimes crescent, sometimes full.

Rumi

I would like to thank the earth, the sea and the sky, and everything and everyone who has lived and died and otherwise engaged in this mysteriously blossoming playground we find ourselves in; I give thanks that together we are so beautifully and endlessly fascinating.

Words cannot express the depth of gratitude I feel for my family. Thank you for supporting me in all that I do. Thank you for reminding me to smile, and to breath, and to laugh, especially when the times felt tough. Thank you, Tracy, Bodhi and Lila, for welcoming me as your friend, your father and your love.

I am grateful for the inspiration of my grandfather George, who instilled in me a love for learning about the workings of this world, and a joyful attitude around the activities of the mind. You will be missed, but not forgotten.

I would like to thank my advisor, Dr. Robert Paasch, for his encouragement and for his counsel. I would like to thank my committee members, Dr. H. Tuba Ozkan-Haller, Dr. Solomon Yim, Dr. Joe Zaworski and Dr. Bart Eleveld, for their insightful comments and critique of this work. I would like to thank all of the faculty who I have had contact with, and who have helped to make my educational experience worthwhile.

I am grateful as well to have been in company of so many bright fellow students. A special thanks goes out to my office mates, with whom I have shared many an intriguing discussion: Adam Brown, Justin Hovland, Kelley Ruehl and Stephen Meicke. Thanks for the good times.

This paper is based upon work supported by the United States Department of Energy under Award Number DE-FG36-08GO18179.

TABLE OF CONTENTS

TABLE OF CONTENTS (Continued)

LIST OF FIGURES

LIST OF FIGURES (Continued)

LIST OF TABLES

LIST OF APPENDIX FIGURES

THE WAVE ENERGY RESOURCE OF THE US PACIFIC NORTHWEST

1. INTRODUCTION

1.1 The nature of the resource

Nearly everything on earth begins with the sun, and ocean waves are no exception. The sun heats the earth unevenly, giving rise to the wind. As the wind blows across vast stretches of sea, ocean waves are generated. The origins of fossil fuels also lie with the sun. However, their availability is the result of millions of years of accumulation and their use constitutes a significant contribution to global climate change. While relatively inexpensive and energy dense fossil fuels account for the majority of the global energy supply today, it is clear that carbon-free, renewable sources must supplant much, if not all, of this. Wind and solar energy conversion technologies have matured over recent decades, and are being installed around the world at an accelerating rate. While ocean wave energy conversion is still unproven on a commercial scale, significant advances in research, design and testing continue to be made. Success will mean access to a resource whose rate of renewal has been estimated to be on the order of 1 to 10 TW (1 TW = 10^{12} W) [1]. Although at most between 10 – 25% of this can likely be converted to electricity [2], this represents a substantial portion of the present global electricity consumption of approximately 2 TW [3].

If we are to harvest energy from ocean waves, we must first understand the resource. While the energy flux of winds or tides involves the gross transport of the medium, the energy flux of ocean waves (to first order) is propagated through the oscillation of the medium. In deep water this energy can travel great distances nearly undiminished, and at any given location there may be waves generated from local winds as well as swell arriving from distant storms. The wave energy resource is highly variable on a scale of months, days or hours; yearly averages tend to

oversimplify this reality. In addition to spatial and temporal variation, at any given point in time and space this energy transport can be seen as the result of a large number of components acting with different directions, amplitudes, phases and periods. The challenge is to reliably and economically convert some portion of the instantaneous mechanical energy comprising this wave energy resource into a more useful form, such as electricity.

1.2 The need for conversion

There are many different ideas for harvesting ocean wave energy, in varying stages of development. The first patent for a wave energy converter was granted in 1799 (Girard and Son, France), and by 2002 over 1000 such patents were held within Japan, Europe and North America [4]. There is no clear indication yet of which devices, or even which basic morphologies, will ultimately be successful. But just as the wind energy industry converged upon the three-blade, horizontal axis turbine it is inevitable that the field of ocean wave energy converters (WECs) will narrow considerably. To better understand the wave energy resource within the context of energy conversion, it will be useful to briefly outline the range of wave energy technologies being pursued today. In-depth reviews of wave energy technology can be found in references such as [2,4,5].

WECs can generally be categorized as either overtopping devices, oscillating water columns or wave activated bodies. It is useful to further classify them as designed for deployment either offshore, near-shore or on the shoreline. *Overtopping devices*, such as the Wave Dragon [6] depicted in Figure 1, are designed to collect water from the crests of incident waves. This water is then allowed to fall through a low-head turbine.

Oscillating water columns (OWCs) consist of an enclosed volume that is partially submerged and open to the sea. The water column rises and falls with the waves, alternately pressurizing and depressurizing a column of air. The resulting airflow drives a e.g. Wells turbine, which spins in one direction regardless of flow

direction. A schematic of a floating OWC from Oceanlinx [7] is presented in Figure 2. An OWC installed on the shoreline of the island of Islay off the coast of Scotland in 2000, the LIMPET [8], is the world's first grid connected WEC (Figure 3).

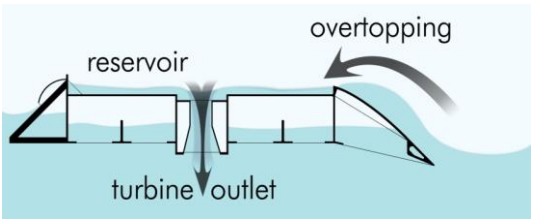

Figure 1. Schematic of Wave Dragon overtopping device [6].

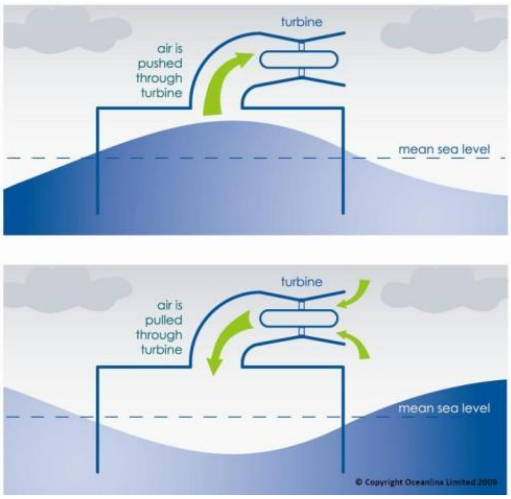

Figure 2. Schematic of Oceanlinx OWC device [7].

Figure 3. LIMPET, a shoreline OWC, developed by Wavegen [9]. In operation since 2000.

Figure 4. The Pelamis attenuator [10].

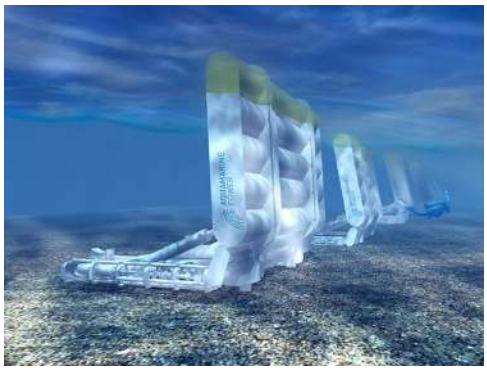

Figure 5. Artist's rendition of the Oyster, a near-shore WEC developed by Aquamarine Power [11].

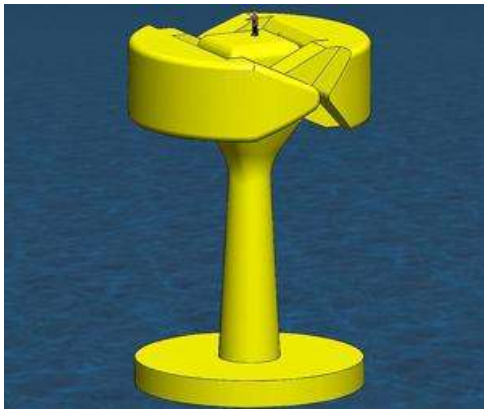

Figure 6. Schematic of a floating WEC, with two pitching bodies, developed by Columbia Power Technologies [12].

Figure 7. The Power Buoy, a heaving point absorber developed by Ocean Power Technologies [13].

Figure 8. Artist's rendition of an array of Archimedes Wave Swing point absorbing WECs [14].

Wave activated bodies (WABs) are excited to motion by the dynamic pressure field associated with ocean wave propagation. Relative motion between multiple bodies, or between a body and a fixed reference such as the sea floor, is harnessed through a variety of means. This may involve compressing a fluid which in turn is

used to drive a generator, a direct drive generator in which a moving magnetic field induces current in a circuit, or some other method.

WABs can be further categorized as attenuators, terminators or point absorbers. An *attenuator* has a length on the order of the incident waves and is oriented parallel to the direction of wave propagation, such that it absorbs energy as the wave passes along its length. An example of an attenuator is the Pelamis [10], shown in Figure 4, where relative motion between sections pressurizes hydraulic fluid. A *terminator* has dimensions similar to an attenuator, but is oriented such that its primary axis is perpendicular to the direction of wave propagation, physically intercepting the waves. A *point absorber* is generally defined as having a characteristic dimension that is much less than the incident wave length. There are many diverse WECs that fall into this category. The Oyster [15], as shown in Figure 5, is a flap-type device that is mounted on the sea floor, and pumps pressurized sea water to an onshore generator. A floating point absorber developed by Columbia Power Technologies [16], shown in Figure 6, activates a direct drive rotary generator with the relative motion of separate fore and aft floating sections. The Power Buoy [13], Figure 7, utilizes the relative motion between a heaving float and a relatively stationary central spar to activate hydraulic machinery. The Archimedes Wave Swing [17], Figure 8, is a completely submerged, bottom-mounted device with a moving section that rises and falls with the pressure differential induced as a wave passes above it.

In the process of developing a WEC, device performance will be optimized within a set of constraints. Rather than maximizing device "efficiency", the goal should be to maximize energy production per unit of monetary expense. Specifics of design principles for WECs are outside of the scope of this research, though fascinating discussion on this subject can be found in references such as [18-20]. Instead, we will briefly outline some of the challenges inherent in harvesting ocean wave energy as context in which to better understand the importance of a robust understanding of the wave energy resource.

To effectively design a robust and survivable ocean wave energy converter, the waves should be seen simultaneously as a resource and a risk and it is imperative that the expected range of conditions be considered when designing and siting WECs. While initial stages of ocean wave energy conversion development tend to assume monochromatic waves traveling in a single direction, the conditions in which the system must eventually operate are random, irregular and directionally divergent.

It is within this harsh, stochastic environment that a WEC must not only convert energy, but also survive. A WEC's performance may be sensitive to a number of quantities characterizing the energy flux, such as wave height, period or direction. Indeed, most devices are designed to operate most effectively in a state of resonance or near-resonance. However, in rough sea states a resonant response may well be catastrophic. A larger generator will be able to take advantage of the dramatically increased wave power resource available during particularly energetic sea states, but will be underutilized the majority of the time. There is also the problem of end-stops: being of finite size, the range of motion of any WEC is necessarily limited and trades between cost and performance must be made. For offshore devices, energy can be expected to arrive from a range of directions, and axisymmetrical device geometry or compliant mooring allowing a reorientation of the device may be necessary to take advantage of the diverse resource. The configuration of an array of devices is not so easily reoriented, and so knowledge of resource directionality will be critical. The intertidal range may have a strong effect on devices that are either tight moored or rigidly anchored to the sea floor, as wave power rapidly attenuates below the surface.

The risks are both long-term (e.g. fatigue, wear and corrosion) and acute (e.g. catastrophic failure during an extreme sea state). To assess long-term risk and reliability a comprehensive characterization of the range of expected sea states is essential. The dynamic behavior of a resonant system in ocean waves is quite complex, and details can be found in e.g. Falnes [21]. In particularly energetic seas, the energy that we seek to exploit can quickly become a liability and the expected performance of a WEC during a 50-year storm, or even a once-a-year storm, must be

investigated thoroughly. It may be necessary for some devices to have a distinct 'survivability mode' in certain conditions, such as constraining relative motion or lowering the device beneath the sea surface. Also, seasonal trends in wave conditions may limit the times in which WECs can be accessed or retrieved for maintenance or repairs. To succeed, a WEC should operate reliably between available maintenance windows, survive infrequent but extreme storm events, and harvest energy over a broad range of sea states sufficient to recover expenses.

1.3 Previous resource assessments

The problem of resource assessment and characterization has been approached in a variety of ways. As will be discussed in Section 2, the stochastic nature of the sea lends itself to analysis in the frequency domain. Large scale resource assessments are typically based upon hindcasts from relatively coarse, global wind-wave models such as WAVEWATCH-III [22] or WAM [23]. Examples include the European Wave Energy Atlas (WERATLAS) [24], an Australian national scale assessment [25] and a global scale wave energy resource assessment [26]. The global distribution of annual mean wave power given by Cornett [26] is reproduced in Figure 9, where it is clear that an abundant wave energy resource exists between the 40° and 60° latitudes, and

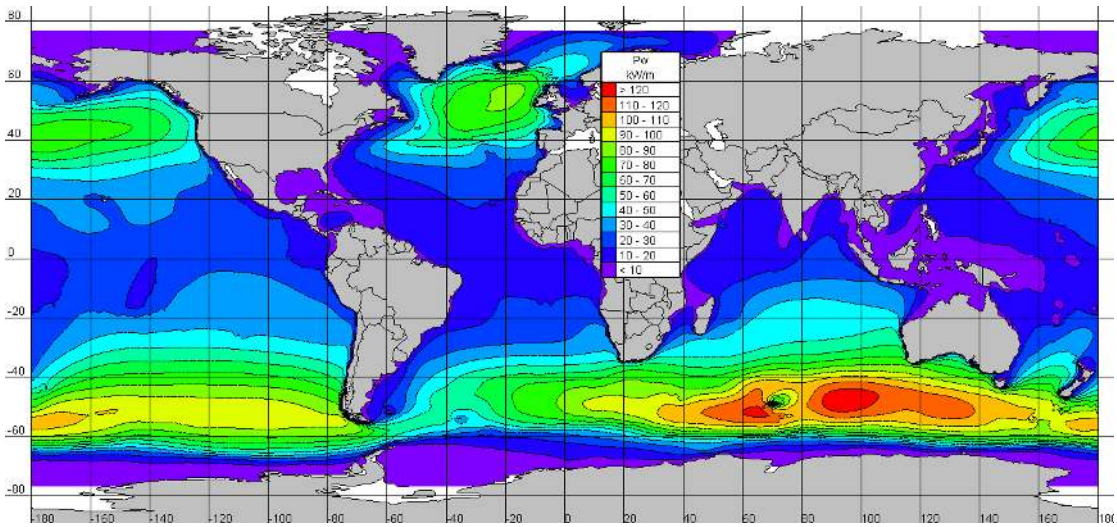

Figure 9. Global distribution of annual mean wave power. (Cornett [26])

along the western coastlines, in both the northern and southern hemispheres.

On a regional or local scale the resource is typically assessed using global or regional wind-wave model data, satellite altimetry, *in situ* measurements (e.g. wave measurement buoys) [27], or a combination of these data sources. Examples include wave energy resource assessments of the UK [28], Portugal [29,30], Sweden [31], Belgium [32], Canada [33] and the Atlantic coast of the southeastern US [34]. Local wave models such as SWAN [35] may be used to numerically model the propagation of sea states across a continental shelf where the bathymetry influences the waves on a finer scale. This has been done in resource assessments of Spain [36,37] and California [38-40]. The primary resource is typically characterized by the energy flux per unit crest width, and additional information may be calculated and reported regarding wave heights, periods and direction.

The Pacific Northwest coast is the most energetic wave resource region in the US, as can be seen by examining Figure 9. Despite this, little has been published regarding the wave energy resource of this region. In 2004 the Electric Power Research Institute (EPRI) published reports surveying potential wave energy development sites in Oregon [41] and Washington [42]. These reports were broadly focused on site selection issues such as grid interties, utility substation capacity and port access, as well as the primary wave resource. Wave measurement buoy and wind-wave model data were utilized for wave energy assessment and the reported results are limited to annual mean wave power estimations at a number grid model output locations and monthly means wave power measurements for one representative location. The present author is unaware of the publication of any comprehensive studies of the wave energy resource covering this region.

The wave energy resource along the coast of California, as mentioned above, has been assessed by Wilson and Beyene [38-40]. They compiled long-term wave statistics (significant wave height, peak period and peak direction) from wave records measured at sites of water depth greater than 100 m. Wave Propagation Transfer Functions were developed using the SWAN model, and used to propagate the ‘tri-

statistics' to grid points spaced 5 km apart within the 100 m depth contour. These characteristic quantities were then used to estimate the wave energy resource within the 100 m contour. The assessment presented in this thesis extends south into Northern California as far as Cape Mendocino (~40 °N lat.) and is in general agreement with the findings of Wilson and Beyene (e.g. mean annual wave power of ~35 kW/m). The present study, while only assessing the resource at wave measurement buoy locations, estimates the wave power using the complete wave spectra (rather than only significant wave height and peak period) and also calculates and reports characteristic quantities describing spectral and directional widths (see Section 4 for details).

1.4 Contribution of this thesis

This study seeks to add to our understanding of the wave energy resource of US Pacific Northwest (Washington, Oregon and Northern California). Archived spectral data from wave measurement buoys at ten locations of varying depths and distances from the coastline form the basis of this comprehensive characterization of the wave energy resource. This study intends to detail the seasonal trends (as well as the variability on the scale of hours and days) of six characteristic quantities describing the wave energy resource, including measures of gross wave power, wave heights, characteristic period, spectral width, characteristic direction and directional uniformity. In addition to temporal variability, the distribution of total energy over these characteristic quantities will be presented. The range of conditions observed in this study reveal much of the character of the wave energy resource in the US Pacific Northwest. Further understanding of the resource is gained by examining persistence statistics, noting how often wave heights remain below some value for at least a given length of time. Finally, a set of representative spectra are proposed. This limited set of spectra can be used to represent the wave climate of the US Pacific Northwest in numerical or physical modeling.

Section 2 introduces linear wave theory and the short-term statistical descriptions of sea states in the frequency domain. Section 3 defines the geographical study area and discusses the data sources used in this study. Also, gaps in the archived spectral records are discussed. In Section 4, the quantities used in this study to characterize sea states are presented and discussed. Section 5 presents the results of the present assessment, as briefly outlined in the preceding paragraph. Conclusions and suggestions for further work are given in Section 6.

2. WAVES AND WAVE ENERGY

2.1 Introduction

If a number of time histories of wave elevation were recorded, each with a slightly different location or start time, none would be the same as any other. However, provided the differences in location and time were small, short-term statistical descriptions of each time history should be in general agreement. While a history of sea surface elevation offers a direct record of wave conditions *for a precise location and time interval*, a spectral analysis of this record yields a probabilistic estimate of the average wave conditions that is valid over tens of minutes and tenths (or tens, in deep water) of kilometers. The characteristics of the waves over this interval of time and space, called the sea state, forms the basis of the present wave energy resource assessment. A real sea state, which is polychromatic and directionally diverse, can be accurately described as the superposition of a large number of long-crested harmonic waves, densely distributed over frequency and direction. To understand the wave energy resource, we must begin by exploring the components of the sea state: harmonic waves.

Section 2.2 will introduce basic harmonic wave mechanics as described by linear wave theory, including the calculation of wave energy flux. Section 2.3 will discuss the description of sea states in the frequency domain. The calculation of quantities characterizing the sea state will be presented in Section 2.4. The account given in the following subsections should be sufficient to understand the methodology and results of this thesis, however a number of excellent texts can provide further details. See, for example, Dean and Dalrymple [43], Holthuijsen [44], Young [45], Tucker and Pitt [27] or Ochi [46] for linear water wave mechanics and spectral analysis of real seas.

2.2 Harmonic waves

Linear wave theory provides a satisfactory description of the mechanics of ocean surface waves over a large majority of conditions. The water wave problem is formulated with the assumptions that the fluid is incompressible, inviscid (and therefore irrotational), allowing the domain to be described by a velocity potential field. The boundary conditions of the resulting partial differential equation are linearized under the assumption of infinitesimal wave amplitude, greatly simplifying the problem. Some basic parameters of the system and its solution are illustrated in Figure 10. The linear wave propagating over water of depth, h, is periodic in space and time with a sinusoidal profile of length, L, amplitude, a, and height, $H = 2a$. Strictly speaking, the linearization is only valid if the wave amplitude is very small in comparison with the wave length and water depth. However, the theory provides suitably accurate predictions in many cases where these assumptions are clearly not met. As waves approach their breaking-limited steepness or propagate into depths where shoaling effects begin to be felt, nonlinearities become more important.

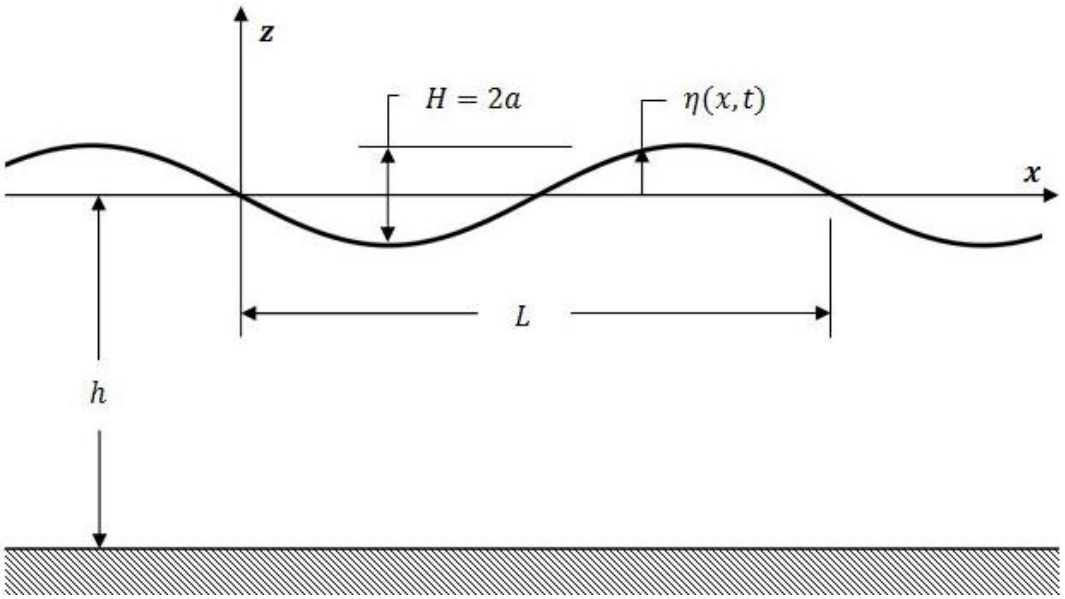

Figure 10. Long-crested, harmonic wave propagating over a horizontal sea floor.

The surface elevation of a harmonic linear wave, called simply a harmonic wave from here on, that is propagating along the x-direction is given by

$$\eta(x,t) = a\cos(kx - \omega t + \phi) \tag{1}$$

where η is the surface elevation at position, x and time, t, $k = 2\pi/L$ is the wave number, L is the wave length, ω is the angular frequency and ϕ is the phase angle.

For a given water depth, the frequency and length of a linear wave are related through the dispersion relation

$$\omega^2 = gk\tanh kh \qquad \text{or} \qquad L = \frac{gT^2}{2\pi}\tanh\left(\frac{2\pi}{L}h\right) \tag{2}$$

where g is the acceleration due to gravity, h is the water depth, and $T = 2\pi/\omega$ is the wave period. The phase speed, or celerity, of a linear wave is the speed at which a wave crest is observed to travel and is calculated as

$$c = \frac{L}{T} = \frac{\omega}{k} = \sqrt{\frac{g}{k}\tanh kh} \tag{3}$$

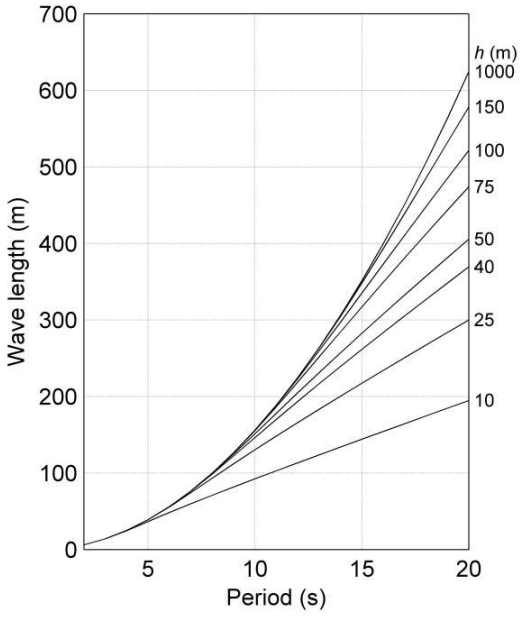

Figure 11. Wave length as a function of period.

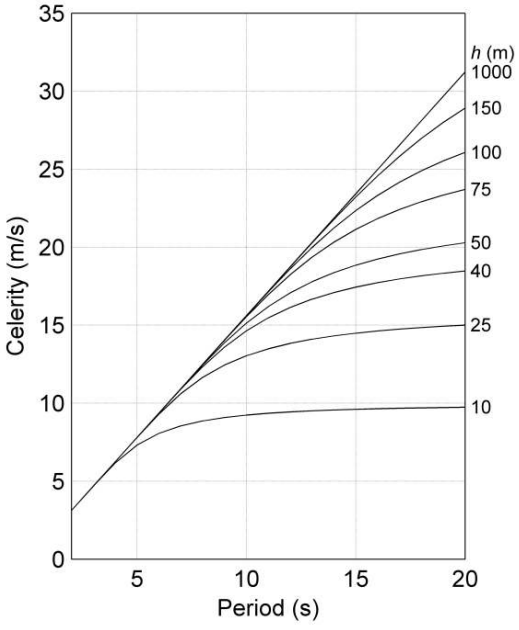

Figure 12. Celerity as a function of period.

where c is the celerity. Wave length and celerity as a function of wave period, at various water depths, are illustrated in Figure 11 and Figure 12, respectively. Outside of shallow water (i.e. water depth less than 1/20 the wave length, or $kh < \pi/10$), where the phase velocity simplifies to a function of only depth, waves of greater period are longer and faster.

It is important to point out that wave energy does not propagate with the wave celerity, but rather with the group velocity. Waves travel in packets, or groups, with waves at the leading edge disappearing and new waves arising at the trailing edge. Outside of shallow water the group speed is less than the phase speed. This frequency dependence of group velocity accounts for the dispersive nature of waves. Winds generate an irregular, polychromatic sea, and the longer period components propagate away faster. This has a filtering affect on the waves that subsequently arrive at a distant location. The resultant narrow-banded seas are called swell, and may occur simultaneously with locally generated wind seas. The group velocity can be calculated as a proportion of the wave celerity as

$$c_g = \left(\frac{1}{2} + \frac{kh}{\sinh 2kh}\right) c \tag{4}$$

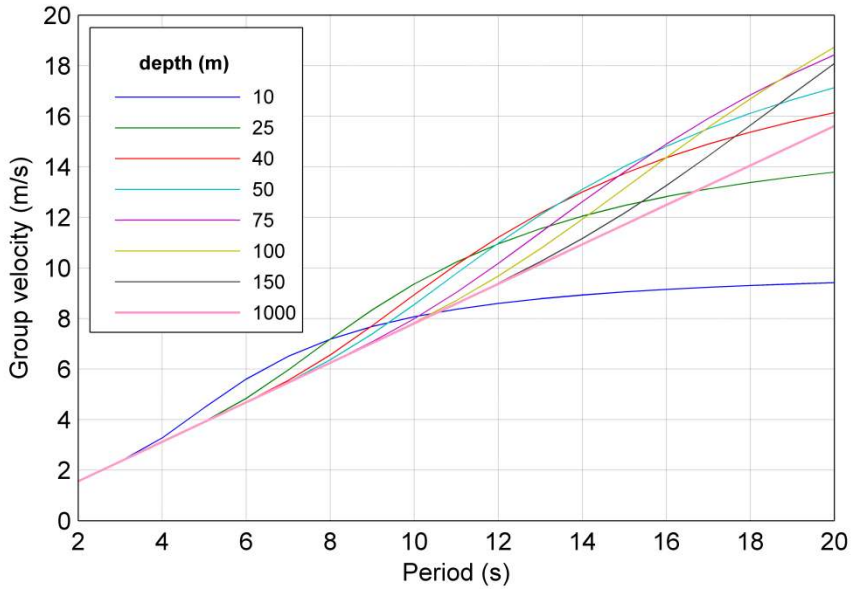

Figure 13. Group velocity as a function of period.

where c_g is the group velocity. Group velocity as a function of wave period, at various water depths, is presented in Figure 13.

In deep water (i.e. water depth greater than ½ the wave length, or $kh > \pi$) the dispersion relation, as well as the calculations of wave celerity and group velocity, are simplified and can be expressed as

$$\omega^2 \approx gk \qquad \text{or} \qquad L_0 \approx \frac{gT^2}{2\pi} \tag{5}$$

$$c_0 = \frac{gT}{2\pi} \tag{6}$$

$$c_{g0} = \frac{1}{2}c_0 = \frac{gT}{4\pi} \tag{7}$$

where L_0 is the deep water wave length, c_0 is the deep water wave celerity and c_{g0} is the deep water group velocity.

There is oscillatory water particle motion associated with propagating waves. The horizontal and vertical components of particle velocity are calculated as

$$u = \omega a \frac{\cosh k(h+z)}{\sinh kh} \cos(kx - \omega t + \phi) \tag{8}$$

$$w = \omega a \frac{\sinh k(h+z)}{\sinh kh} \sin(kx - \omega t + \phi) \tag{9}$$

where u and w are the horizontal and vertical components of particle velocity, respectively. It is clear that these components of velocity are 90° out of phase, with u being in phase with surface elevation, η. Additionally, the magnitude of the oscillatory motion decays with water depth. Note that the rate of decay is greater for shorter waves. Velocity vectors under harmonic waves of two different periods are shown in Figure 14.

The pressure field associated with a propagating harmonic wave is the sum of the hydrostatic pressure of the undisturbed fluid and the dynamic pressure

$$p = -\rho g z + p_D \tag{10}$$

$$p_D = \rho g \eta \frac{\cosh k(h+z)}{\cosh kh} \tag{11}$$

where p is the total pressure, p_D is the dynamic pressure and ρ is the density of sea water. The dynamic pressure is the result of hydrostatic pressure due to the displacement of the free surface, as well as vertical component of particle acceleration, which is 180° out of phase with the free surface. It is seen that the dynamic pressure is hydrostatic at $z = 0$ (i.e. $\rho g \eta$), and that further down the water column it is reduced by the pressure response factor (i.e. the fourth multiplicand of Eq. 11). It is the total pressure field that determines the hydrodynamic forces on a WEC (if we disregard the effects of viscosity), although this pressure field is modified by the presence of a body (e.g. diffraction) and the body's motion (e.g. radiation). Details on the dynamics of ocean structures can be found, for example, in the texts of Falnes [21] or Chakrabarti [47].

There is kinetic and potential energy associated with particle motion and displacement of the free surface, respectively. The average total energy per unit surface area associated with a linear wave can be shown to be equal to

$$E = \frac{1}{2}\rho g a^2 \tag{12}$$

where E is the average energy per unit surface area. Several important points need to be made here. First, the average kinetic energy and potential energy contribute

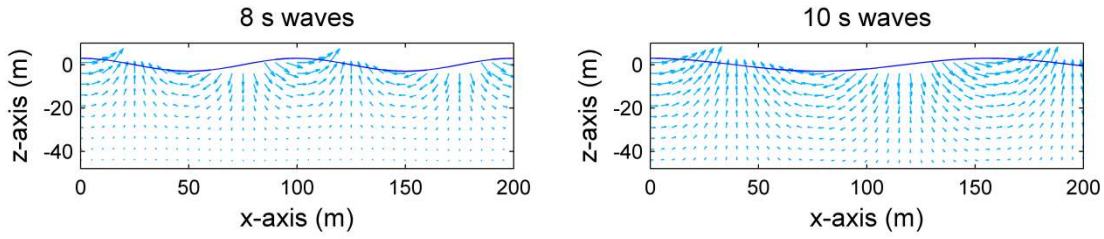

Figure 14. Particle velocity vectors. Harmonic wave trains propagating to the right, at an instant in time. Influence of longer 10 s waves extends deeper into water column.

equally to the total energy over an integral number of wave lengths. Secondly, neither water depth nor wave length influence the total energy. Finally, the energy is proportional to the variance of the surface elevation of the wave. Recall that variance is the average squared deviation from the mean, and that for a harmonic wave form the variance is equal to half the amplitude squared, $a^2/2$. This will be important to keep in mind when later we use spectral analysis and the variance density spectrum to characterize polychromatic seas.

There is no gross transport of mass associated with the propagation of linear waves; it is energy that is being transported. The rate of energy transport through an area is the energy flux, and according to linear theory it is the rate of work done by the fluid on one side of an envisioned vertical plane to the fluid on the other side. Of course it is only the horizontal motion of the water particles that can contribute to work done at a vertical plane, and so the energy flux per unit width of crest, from the sea floor to the sea surface and averaged over one wave period, for an undisturbed linear wave, is calculated as

$$J = \frac{1}{T}\int_{t}^{t+T}\int_{-h}^{\eta} p_D\, u\; dz\, dt \tag{13}$$

where J is the average energy flux per unit crest width, also called the average wave power, and t indicates time. As we will not look into instantaneous energy flux in this study, an average value will be assumed when either energy flux or wave power is used.

It can be shown, retaining terms to the second order in wave height, that the wave power of a harmonic, linear wave calculated in Eq. 13 can be expressed as

$$J = \frac{1}{2}\rho g a^2 c_g = E c_g \tag{14}$$

Thus, the energy flux per unit crest width is equal to the total energy per unit surface area, transported at the group velocity. This wave power, typically expressed in units of kW/m, is the primary resource that we seek to harvest a portion of using WEC

technology. Note that while the wave energy is dependent only upon the amplitude of the wave, the group velocity and thus the wave power is dependent upon the wave length and the water depth.

2.3 Wave spectra and sea states

When the wind blows across the surface of sea, waves are generated. Although these waves generally propagate in the direction of the wind, water waves tend to be directionally spread about this primary direction. Aside from energy input by the wind, there are wave-wave interactions in which energy is transferred between components of different frequencies and directions. Energy is dissipated through breaking waves and, outside of deep water, through friction at the sea floor. The waves can feel the bottom when they are outside of deep water, and will turn to orient their direction of propagation perpendicular to the bathymetric contours in a process called

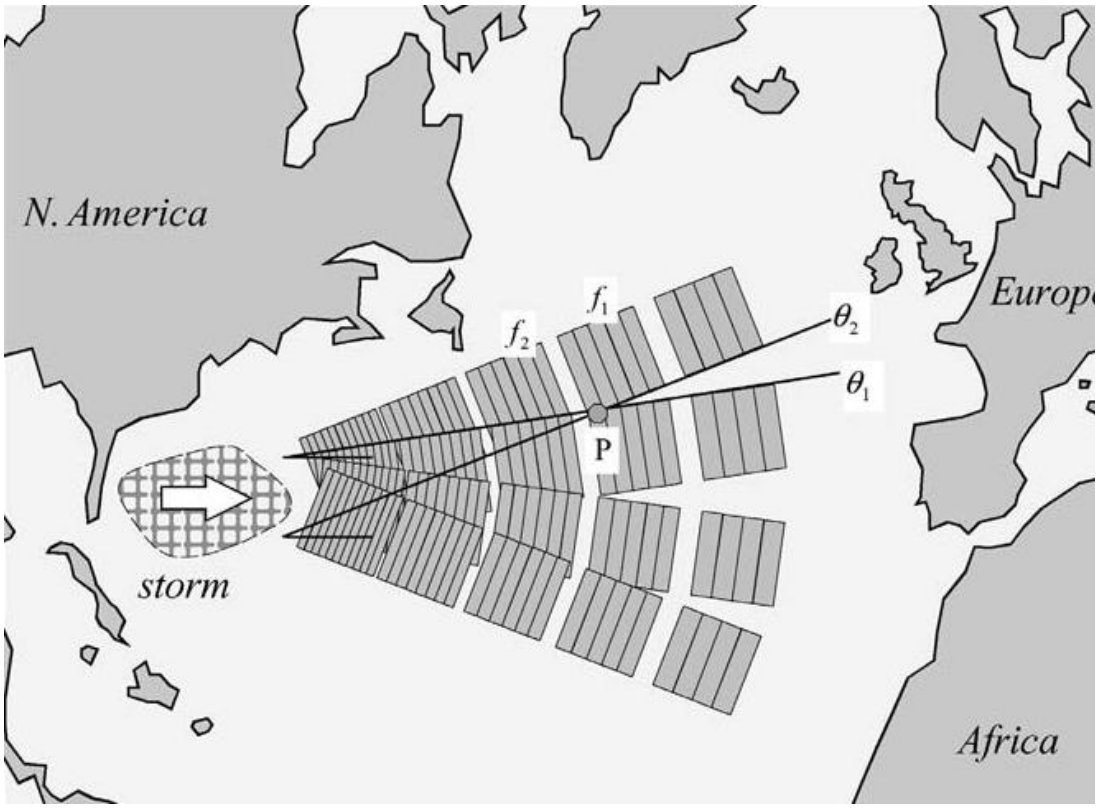

Figure 15. Filtering of wave energy by spectral and directional dispersion. (Holthuijsen [44])

refraction. Far away from the region of generation, spectral and directional dispersion will have acted to filter the wave energy. A narrow range of frequencies and directions will have separated from the rest of system, as illustrated in Figure 15, and are known as swell.

At any particular time and place at sea, ocean wave energy will propagate with a range of frequencies and directions. Some of the waves may have been generated by local winds, and some may have travelled from distant storms. The variance of sea surface elevation distributed over frequency is known as the variance density spectrum, $S(f)$, or simply the spectrum. As the waves do not all propagate in a single direction, the variance can also be distributed over both frequency and direction, $S(f,\theta)$, in which case it may be called the frequency-directional variance density spectrum, or simply the directional spectrum.

If the conditions are stationary and ergodic, and the sea surface elevation follows a Gaussian distribution, then the variance density provides a complete, short term statistical description of the ocean waves. Conditions can generally be assumed to be stationary over a period of 15 minutes to several hours. Ergodicity can be assumed if the bathymetry does not change too rapidly. The Gaussian distribution of elevation follows from our assumption of linear waves. As long as wave amplitudes are small in comparison to water depth and wave length, wave components do not interact with one another and their phases are randomly distributed. Under these assumptions, the sea can be considered as the superposition of an infinite number of wave components, densely distributed over frequency and direction, with phases uniformly distributed over the interval $[0, 2\pi]$.

In practice, a finite number of discrete components can be used to describe the sea. If the variance is discretely distributed over frequency and direction, then the sea surface can be described as

$$\eta(x,y,t) = \sum_{i,j} a_{ij} \cos\left(k_i(x\cos\theta_j + y\sin\theta_j) - 2\pi f_i t + \phi_{ij}\right) \qquad (15)$$

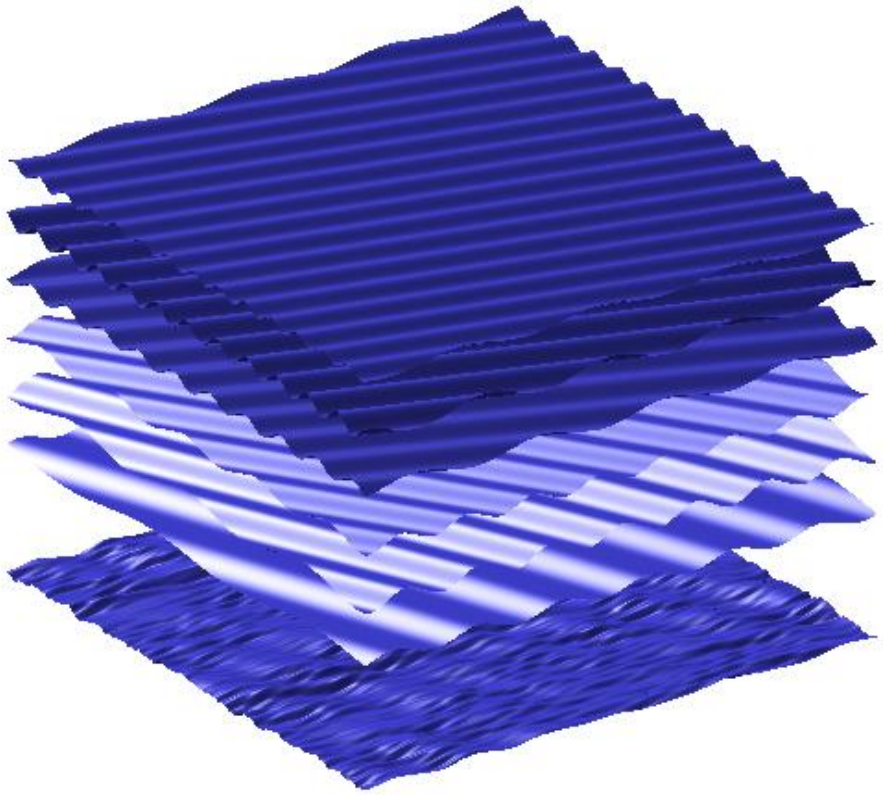

Figure 16. Polychromatic directional sea as the superposition of long-crested, harmonic waves. In the interest of clarity, not all components are shown.

where $f_i = \omega_i/2\pi$ is the i^{th} discrete frequency, θ_j is the j^{th} discrete direction, a_{ij} and ϕ_{ij} are the amplitude and phase associated with the component with frequency, f_i and direction, θ_j and the wave number k_i is found through the dispersion relation (Eq. 2). Figure 16 illustrates the synthesis of a polychromatic, directionally spread sea from a number of harmonic, unidirectional wave components. Under the assumption of linearity, not only can the elevations of these wave components be superposed, but also the particle velocities and dynamic pressures.

Recalling that the variance of a harmonic wave is equal to $a^2/2$, if the variance density for a given frequency and direction is known then the corresponding component amplitude is determined as

$$a_{ij} = \sqrt{2\, S_{ij}\, \Delta f_i \Delta \theta_j} \tag{16}$$

where S_{ij} is the variance density for the i^{th} discrete frequency and j^{th} discrete direction, Δf_i is frequency width of the discrete distribution centered at f_i, and $\Delta \theta_j$ is the directional width of the discrete distribution centered at θ_j. As stated earlier, the phases of each component are uniformly distributed on the interval $[0, 2\pi]$.

The frequency variance density can be obtained from the frequency-directional variance density by summing over direction

$$S_i = \sum_j S_{ij}\, \Delta \theta_j \tag{17}$$

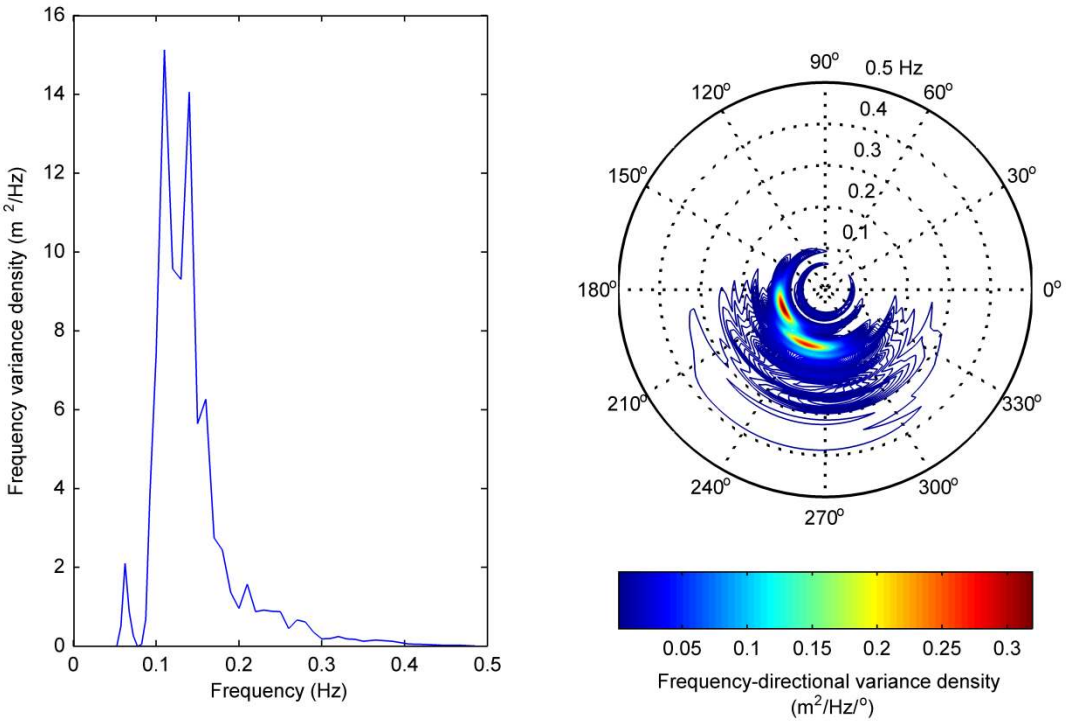

Figure 17. Frequency and frequency-directional spectra representing a single sea state. Measured by Col River Bar data buoy in November 2008. Following convention, the frequency-directional spectrum indicates the direction from which waves are arriving.

where S_i is the frequency variance density for the i^{th} discrete frequency. Similarly, the frequency-directional variance density is related to the frequency variance density by the directional spreading function

$$S_{ij} = S_i D_{ij} \tag{18}$$

where $D_{ij} = D(f_i, \theta_j)$ is the directional spreading function. The directional spreading function is non-zero and has the property $\sum_j D_{ij} = 1$.

To describe the sea in the frequency domain, variance spectra must be estimated using measurement and/or wind-wave modeling. This study made use of archived spectra from wave measurement buoys, as described in the following section. By way of example, the frequency density spectrum and frequency-directional density spectrum of one sea state are shown in Figure 17.

3. WAVE DATA

3.1 Sources of wave data

Under investigation is the wave energy resource off the coasts of Washington, Oregon and northern California, an area bounded by 40-49 °N latitudes and 124-125 °W longitudes. For the purpose of this characterization, the surface of the sea is regarded as a Gaussian random process under the assumptions of stationarity and ergodicity. This, along with an assumption of small amplitude linear wave theory, allows a descriptive analysis of sea states in the frequency domain.

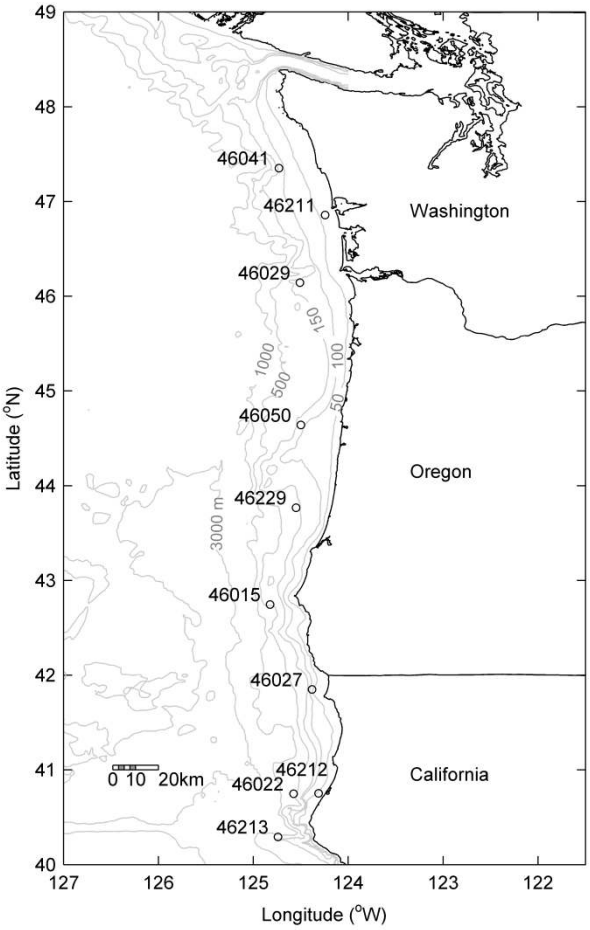

Figure 18. Locations of wave measurement buoys utilized in this study.

Archived spectral records from wave measurement buoys were used in this assessment. The records were obtained from the websites of both the National Data Buoy Center (NDBC - www.ndbc.noaa.gov) and the Coastal Data Information Program (CDIP – www.cdip.ucsd.edu), each of which operates and maintains a network of wave measurement buoys. The locations of the buoys considered in this study are provided in Figure 18. For consistency, all buoys are referred to using their NDBC station ID numbers. It has become standard practice to archive the variance spectral density as a discrete function of frequency, but prior to this NDBC simply reported a few quantities derived from the spectrum, such as significant wave height and peak period. Although these quantities can be used to estimate the energy flux, nothing is revealed about the distribution of this energy flux over frequency or direction. To examine the complexity of the sea states of the Pacific Northwest only those records which archived the variance spectral density were used, from their earliest availability through the end of 2008. For the 10 buoys used in this study, this provided over 700,000 hourly records of spectral density, with information on the directional distribution provided for over 400,000 of these records. The names and locations of the buoys, as well as the availability of their spectral records, are provided in Tables 1 and 2.

All NDBC stations used in this study are currently taking directional wave measurements using a pitch-roll-heave payload housed in a 3 meter discus buoy, and archive spectral records once every hour. CDIP archives spectral records every half an hour, and the buoys included in this study are 0.9 meter directional Waverider buoys. Prior to 1998, CDIP records were processed and archived at varying time intervals, often every 3 or 6 hours. For consistency in comparison alongside the hourly NDBC records, where two CDIP records are available during the same nominal clock hour they have been averaged. More information on the buoy data programs can be found in the following references for NDBC [48,49] and CDIP [50]. Detailed information about wave measurement buoys and spectral analysis can be found in Tucker and Pitt [27].

After being compiled in a common format, each record consisted of a discrete listing of frequency, f_i, frequency bin width, Δf_i, and the variance density, S_i, where i is an index signifying the i^{th} discrete frequency. Although varying with the program as well as the year, there were typically between 38 and 64 discrete frequencies

Table 1. List of wave measurement buoys.

Station ID	Station name	Program	Lat. (°N), Long. (°W)	Mean depth (m)	Distance to shore (km)
46041	Cape Elizabeth	NDBC	47.35, 124.73	132	30
46211	Grays Harbor	CDIP	46.86, 124.24	40	9
46029	Col River Bar	NDBC	46.14, 124.51	135	40
46050	Stonewall Banks	NDBC	44.64, 124.50	123	34
46229	Umpqua Offshore	CDIP	43.77, 124.55	186	30
46015	Port Orford	NDBC	42.75, 124.82	422	24
46027	St Georges	NDBC	41.85, 124.38	48	13
46212	Humboldt Bay S. Spit	CDIP	40.75, 124.31	40	6
46022	Eel River	NDBC	40.75, 124.58	630	26
46213	Cape Mendocino	CDIP	40.29, 124.74	325	33

Table 2. Intervals over which frequency spectral data and frequency-directional spectral data were analyzed. The proportions of hours with data over the analyzed intervals are included.

Station ID	Spectral data interval	Proportion with spectral data	Directional spectral data interval	Proportion with directional spectral data	Duration of sample (s)
46041	1996-2008	0.68	1998-2008	0.69	2400
46211	1987-2008	0.64 (0.93[a])	1993-2008	0.81 (0.93[a])	1600[b]
46029	1999-2008	0.86	1999-2008	0.78	1200
46050	1996-2008	0.80	2008-2008	0.98	1200
46229	2006-2008	0.99	2006-2008	0.99	1600[b]
46015	2002-2008	0.76	2007-2008	0.74	1200
46027	1996-2008	0.73	2005-2008	0.73	2400
46212	2004-2008	0.97	2004-2008	0.97	1600[b]
46022	1996-2008	0.81	2007-2008	0.93	1200
46213	2004-2008	0.94	2004-2008	0.94	1600[b]

[a] Proportion of hours with data from 1998 to 2008.
[b] For CDIP half-hourly records, where two records were begun in the same nominal hour, the two spectra were averaged together resulting in a total duration of 3200 seconds.

ranging from 0.02 to 0.5 Hz. The directional records also included the directions, $\theta_{n,i}$, and normalized magnitudes, $C_{n,i}$, of the first two harmonics of the Fourier series estimation of the directional spreading function. Here $n = 1, 2$ and signifies the first or second harmonic, and θ indicates the direction of wave propagation measured counter-clockwise from east, such that waves approaching from due south would be associated with $\theta = 90°$. Note that θ, the direction of wave propagation, differs by 180° from the direction indicated in Figure 17, where the direction from which waves arrive is represented. These directional parameters were used to estimate the frequency-directional variance spectrum, as outlined in Section 3.2.

3.2 Estimating the frequency-directional variance density spectrum

The frequency variance density is provided by the archived records. However, only a limited number of directional parameters are available for estimating the directional spreading function (and thus the frequency-directional variance density, see Eq. 18). An excellent survey of methods used in estimating the frequency-directional variance density is provided by Benoit et al. [51]. This study employs the relatively low-resolution, but computationally efficient, cos-2s model in which the directional spreading function is estimated as

$$D_{ij} = F(s_i) \left| \cos \frac{\theta_j - \theta_{1,i}}{2} \right|^{2s_i} \tag{19}$$

$$F(s_i) = \frac{2^{2s_i - 1}}{\pi} \frac{\left(\Gamma(s_i + 1)\right)^2}{\Gamma(2s_i + 1)} \tag{20}$$

where s_i is a frequency-dependant parameter describing the spreading of energy about a spectral mean direction (i.e. $\theta_{1,i}$), θ_j is a discrete direction and F is a normalizing function such that $\sum_j D_{ij}\, \Delta\theta_j = 1$. A total of 128 directional bins were used to discretize direction. The spreading index, s, was taken as the arithmetic mean of the spreading indices derived from the first two harmonics [52]

$$s_{1,i} = \frac{C_{1,i}}{1 - C_{1,i}} \tag{21}$$

$$s_{2,i} = \frac{1 + 3C_{2,i} + \sqrt{1 + 14C_{2,i} + C_{2,i}^2}}{2(1 - C_{2,i})} \tag{22}$$

$$s_i = \frac{s_{1,i} + s_{2,i}}{2} \tag{23}$$

At a given frequency, the cos-2s model imposes a symmetric and unimodal (see Figure 19) directional spreading function that may not be accurate in all cases. Bimodal (i.e. two peaked) directional distributions may be evident when, for instance, the wind suddenly shifts direction or swell systems of similar frequencies arrive from different, far away storms. Although it is possible to resolve directionally bimodal systems (for example, using the Extended Maximum Entropy Method [51]), the increased computational effort is likely not justified for the purposes of this resource characterization.

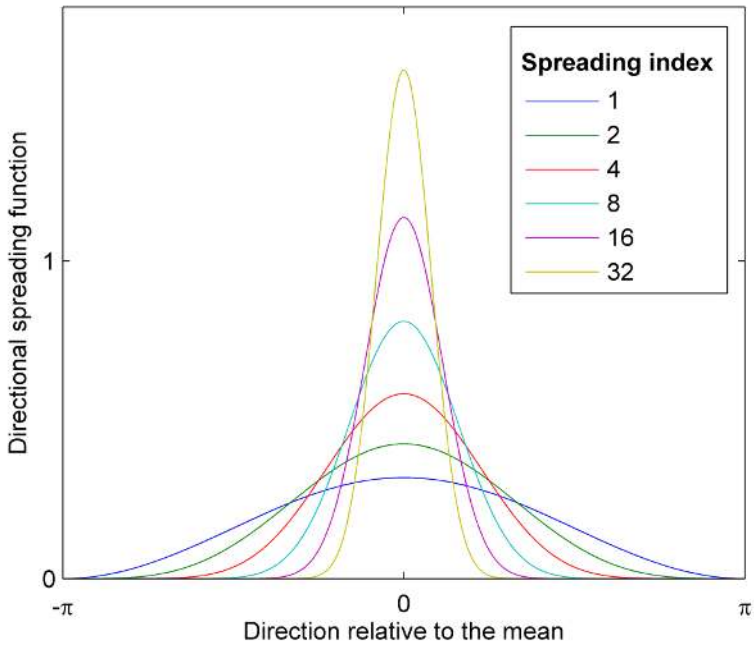

Figure 19. Directional spreading function using the cos-2s model.

3.3 Gaps in the records

An unavoidable downside to utilizing buoy measurements is the prevalence of gaps in the records. These are often due to data transmission errors, planned maintenance or device failure. A considerable number of small gaps of a few hours or less exist, but more importantly there are occasionally periods of several months to a year when no records are available. For most of the buoys examined in this study, a significant majority of the missing records were from the winter and spring months. Presumably much of this is due to the energetic seas of the winter months leading to more failures, as well as an inability to retrieve, repair and redeploy the buoys during these conditions. The distribution of missing records by gap length, for station 46029, is presented in Figure 20, along with the availability of records for each month.

To avoid bias away from periods when more records were missing, each

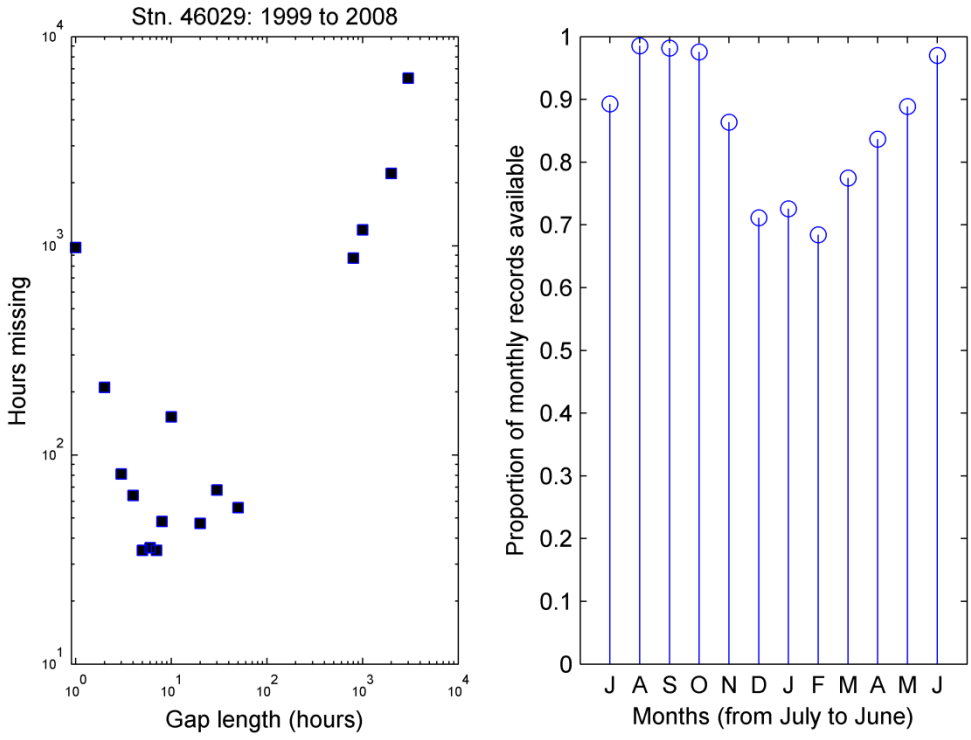

Figure 20. Distribution of missing records, and monthly availability of records, for station 46029.

buoy's records were weighted such that the appropriate number of hours for each of the 12 months was represented. In other words, if a total of *N* hourly records were available for a month of *D* days over a period of *Y* years, then each available record within that month was assumed to occur a total of 24**D***Y*/*N* times. This weighting is simply the inverse of the monthly availability displayed in Figure 20.

4. CHARACTERIZATION OF SEA STATES

Each spectral record was assumed to depict the distribution of variance over frequency (and direction for directional records) for a period of 1 hour, though this was modified by the weighting described in Section 3.3. Of primary interest is the determination of the omnidirectional (i.e. directionally unresolved) wave energy flux per unit width, or wave power, as this is a base measure of the primary resource. Of course, any WEC must be able to convert the resource to useful work, and must be able to survive both fatigue and extreme loading. Consequently, we are interested in further describing the sea states in which a WEC interacts with this primary resource. Six quantities were calculated from each hourly spectrum to characterize not only the wave power itself, but also the wave heights and the distribution of energy over frequency and direction. For the earlier records where the variance is distributed only over frequency, quantities describing directionality were not calculated. These six quantities, described in the following subsections, are

- omnidirectional wave power,
- significant wave height,
- energy period,
- spectral width,
- direction of the maximum directionally resolved wave power, and
- directionality coefficient.

One approach to representing sea states is to fit each measured spectra to a theoretical shape, such as the Pierson-Moskowitz or JONSWAP spectra (see e.g. [27]). Kerbiriou et al. [53] show that, due to the prevalence of mixed sea-swell systems, a single unimodal model spectrum can lead to erroneous results in energy flux calculations, and that improved accuracy can result by partitioning mixed sea states into two or more separate systems. The present study bypasses this issue by considering the discrete spectrum of each sea state as it is measured, and makes no attempt to partition wave systems or use spectral models.

4.1 Characteristics of the total sea state

According to frequency domain analysis and linear wave theory, a real sea can be described by the superposition of an infinite number of long-crested, harmonic waves of different frequency, amplitude, direction and phase. In practice, spectral estimates for a finite number of discrete frequencies are available, with the resolution limited in the first place by the sampling duration, and again when averaging to smooth the spectrum.

The wave power of a long-crested sinusoidal wave is proportional to its variance (i.e. $a^2/2$), as shown in Eq. 14. The omnidirectional wave power of a polychromatic sea is found by summing the contributions to wave power of each of the component waves described by the discrete wave spectrum

$$J = \sum_{i,j} \rho g c_{g,i} S_{ij} \Delta f_i \Delta\theta_j = \sum_{i} \rho g c_{g,i} S_i \Delta f_i \tag{24}$$

where $c_{g,i}$ is the group velocity at the i^{th} frequency and the total variance at frequency f_i is $S_i \Delta f_i = S_{ij} \Delta f_i \Delta\theta_j = a_i^2/2$. J is the total wave power, regardless of direction, and can be seen as the energy flux through a vertical cylinder of unit diameter, extending from the sea floor to the surface.

The significant wave height, H_s, is a characteristic wave height commonly used to describe a given sea state. Strictly speaking, H_s is defined as the average height of the highest 1/3 of zero crossing waves for a given sample and is determined by analysis of a surface elevation record. The significant wave height can be estimated from the frequency domain as

$$H_{m0} = 4\sqrt{m_0} \tag{25}$$

where H_{m0} is the spectral estimate of significant wave height and m_0 is the zeroeth moment of the variance spectrum. The n^{th} order moments of the variance spectrum are calculated as

$$m_n = \sum_i f_i^n S_i \Delta f_i \tag{26}$$

where m_n is the spectral moment of n^{th} order. This spectral estimation of significant wave height assumes a Rayleigh distribution of zero crossing wave heights, and thus a distribution of variance over a very narrow band of frequencies. In real seas H_{m0} overestimates H_s by 1.5 to 8% [46]. In the present study, the spectral estimate is used to characterize the expected wave heights of a given sea state, and significant wave height will from here on be understood to refer to H_{m0}.

4.2 Characteristics of frequency

In a real sea, the variance is distributed over frequency and the response of a WEC will vary with this distribution. As the sea often includes multiple wave systems (e.g. locally generated wind sea and remotely generated swell), and the shape of the frequency variance density spectrum is not known *a priori*, quantities calculated using the entire spectrum may be more robust descriptors than the peak frequency. A characteristic period and a measure of spectral width can be defined, respectively, as the weighted average and the proportional standard deviation of the spectral scale. In fact, similar measures of mean and width can be calculated using either variance or wave power density on the ordinate, and with either frequency or period along the abscissa. Figure 21 shows one sea state represented in these four ways, with means and standard deviations indicated.

Calculating such a mean and width using the variance distributed over frequency, $S(f)$, we arrive at the so-called mean period [27] and a measure of spectral width first suggested by Longuet-Higgins [54]

$$T_{01} = \frac{m_0}{m_1} = \frac{\sum_i S_i \Delta f_i}{\sum_i f_i S_i \Delta f_i} \tag{27}$$

$$\nu = \frac{\sqrt{\frac{m_2}{m_0} - \left(\frac{m_1}{m_0}\right)^2}}{\frac{m_1}{m_0}} = \sqrt{\frac{m_0 m_2}{m_1^2} - 1} \tag{28}$$

where T_{01} is the mean period and ν is a measure of spectral width.

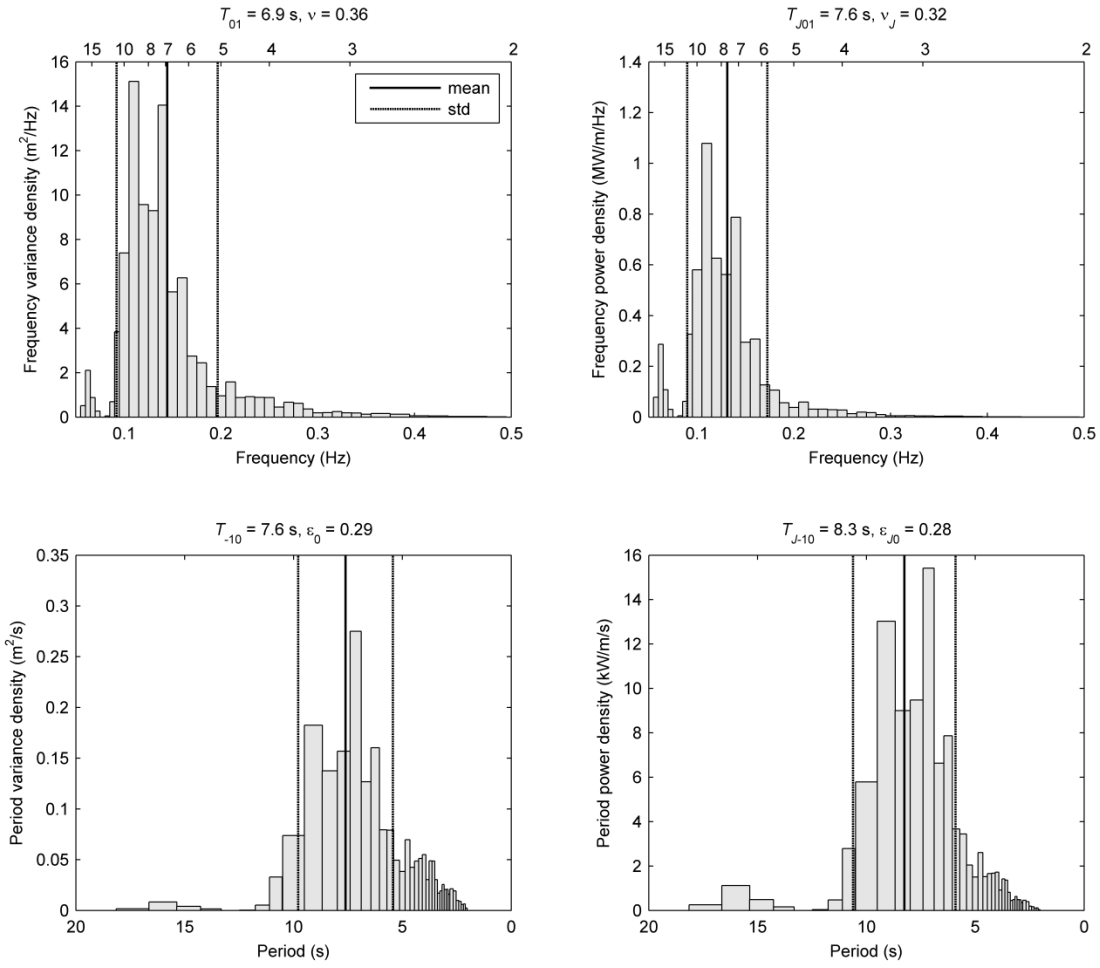

Figure 21. Four discrete representations of a single sea state. They are depicted using frequency variance density, $S(f)$, period variance density, $S(T)$, frequency power density, $J(f)$, and period power density, $J(T)$. The area of each rectangle represents a portion of either the total variance (for the two spectra on the left) or the total wave power (for the two spectra on the right). A characteristic period and spectral width is indicated above each representation.

If the calculations are made using the variance distributed over period, $S(T)$, the relatively powerful, lower frequency components are emphasized. This is a result of a lengthening and shortening of low and high frequency moment arms, respectively, compared to $S(f)$. Here we have the energy period and a measure of spectral width that were first suggested by Mollison [55] and calculated as

$$T_e \equiv T_{-10} = \frac{m_{-1}}{m_0} = \frac{\sum_i f_i^{-1} S_i \Delta f_i}{\sum_i S_i \Delta f_i} = \frac{\sum_i T_i S_i \Delta f_i}{\sum_i S_i \Delta f_i} \tag{29}$$

$$\epsilon_0 = \sqrt{\frac{m_0 m_{-2}}{m_{-1}^2} - 1} \tag{30}$$

where T_e or T_{-10} is the energy period and ϵ_0 is a measure of spectral width. T_{-10} is widely used within the wave energy community, and ϵ_0 has been shown to correlate well to power performance for some WECs [56,57]. The present study uses T_{-10} and ϵ_0 to characterize the frequency distribution of individual sea states. Most WECs are designed as resonant devices that operate most effectively when the excitation frequency approaches some optimum value and thus the central value and the width of the spectrum are expected to play a large role in their response [21].

As we are interested in understanding the wave power resource, the two power spectral densities illustrated in Figure 21 are worth investigating. Although not shown here, the spectral width of the frequency power spectrum, $J(f)$, was found to be quite sensitive to high frequency cutoff, and the mean period of the period power spectrum, $J(T)$, was found to not correlate with omnidirectional wave power as well as T_{-10}. Interestingly, T_{-10} may provide a satisfying characterization of the mean period for the wave energy community because it is identical, in deep water, to the weighted center of the wave power distributed over frequency, $J(f)$. Making use of the deep water approximation for group velocity (Eq. 7), the moments of the power spectrum can be approximated in deep water as

$$m_{Jn} = \rho g \sum_i f_i^n c_{g,i} S_i \Delta f_i$$
$$\cong \rho g \sum_i f_i^n \left(\frac{g}{4\pi f_i}\right) S_i \Delta f_i = \frac{\rho g^2}{4\pi} \sum_i f_i^{n-1} S_i \Delta f_i = \frac{\rho g^2}{4\pi} m_{n-1} \quad (31)$$

and thus

$$T_{J01} = \frac{m_{J0}}{m_{J1}} \cong \frac{m_{-1}}{m_0} = T_{-10} \quad (32)$$

where m_{Jn} is the n^{th} moment of the power spectral density and T_{J01} is its weighted center.

4.3 Characteristics of direction

The quantities used in this study to characterize the directionality of an individual sea state are the direction of the maximum directionally resolved wave power and the directionality coefficient. The frequency-directional variance density, estimated in Section 3.2, is used to calculate the frequency-directional power density

$$J_{ij} = \rho g c_{g,i} S_{ij} \quad (33)$$

The directionally resolved wave power propagating in direction θ, or the energy flux per unit width passing through a vertical plane extending from the sea floor to the surface and whose normal points in direction θ, can be calculated by resolving the wave power of each component in direction θ

$$J_\theta = \sum_{i,j} J_{ij} \Delta f_i \Delta\theta_j \cos(\theta - \theta_j)\delta \qquad \begin{cases} \delta = 1, & \cos(\theta - \theta_j) \geq 0 \\ \delta = 0, & \cos(\theta - \theta_j) < 0 \end{cases} \quad (34)$$

where J_θ is the directionally resolved wave power propagating in direction θ and δ ensures that only positive valued components contribute to J_θ. As pointed out by Mollison [55], according to linear wave theory waves travelling in opposite directions pass through one another unchanged. A vector sum of the wave power of all harmonic wave components is often used to determine the maximum directionally resolved

wave power (see e.g. [58]). This vector sum method cancels components of wave power propagating in opposing directions, typically resulting in an under prediction of directionally resolved wave power of less 3%, for the stations in this study. Although this error is small compared to the uncertainties inherent in the estimation of the spectrum, the more rigorous method presented in Eq. 34 was used in the present work.

The maximum directionally resolved wave power is designated as J_{θ_J}. The direction associated with J_{θ_J} is θ_J and is used as the characteristic direction of the sea state. The directionality coefficient is the ratio of the maximum directionally resolved wave power to the omnidirectional wave power [55]

$$d_\theta = \frac{J_{\theta_J}}{J} \tag{35}$$

where d_θ is the directionality coefficient, representing the degree to which the wave power of a sea state follows a common direction. Unlike the spectral width, where a large value indicates a broad spectral spread, a large directionality coefficient signifies a narrow directional spread.

θ_J and d_θ are likely to be important characteristics for directionally sensitive WECs of fixed orientation, as well as for arrays of WECs of any type. θ_J may not be important for a single, directionally sensitive WEC that can 'weathervane' into the prevailing waves, however d_θ is still likely to influence its performance.

5. WAVE ENERGY RESOURCE OF THE US PACIFIC NORTHWEST

5.1 Seasonal trends

To gain a high level understanding of the energy flux and associated sea states occurring at each wave measurement buoy location, the time-weighted mean characteristic quantities were calculated over the periods for which records were analyzed. These average values reveal much about the suitability of a location, or region, for wave energy conversion, though by themselves they necessarily obscure the variability inherent in the sea. To provide a sense of the typically occurring range of each of these quantities, the 1/6 and 5/6 quantiles (i.e. 17% and 86%) were also calculated. These values represent the limits of the range over which each characteristic quantity was observed 2/3 of the time. The mean values and 2/3 ranges for each buoy location are presented in Figure 22 on an annual basis, as well as for the winter months (defined as December through February) and the summer months (defined as June through August).

Some strong seasonal trends can be seen in these plots, with wave power and significant wave heights much greater in the winter months than in the summer months. Averaged over all 10 stations, the mean wave power is 36 kW/m annually, 64 kW/m during the winter months and 12 kW/m in the summer months. At some locations, the mean wave power during the winter months is over 7 times that of the mean during the summer months. Significant wave height follows a similar trend with a mean of 2.4 m annually, 3.1 m during the winter and 1.6 m during the summer. Winter months are also typified by sea states with a higher energy period (9 s averaged over the year, 10.5 s during the winter and 7.5 s in the summer), a narrower spectral width and an increased directionality coefficient. These differences are likely due, in part, to the prevalence of relatively narrow-banded, powerful swell arriving from distant winter storms. The direction of maximum directionally resolved wave power tends to head more to the south in the summer months (i.e. the value of θ is reduced), swinging around towards the north in the winter months.

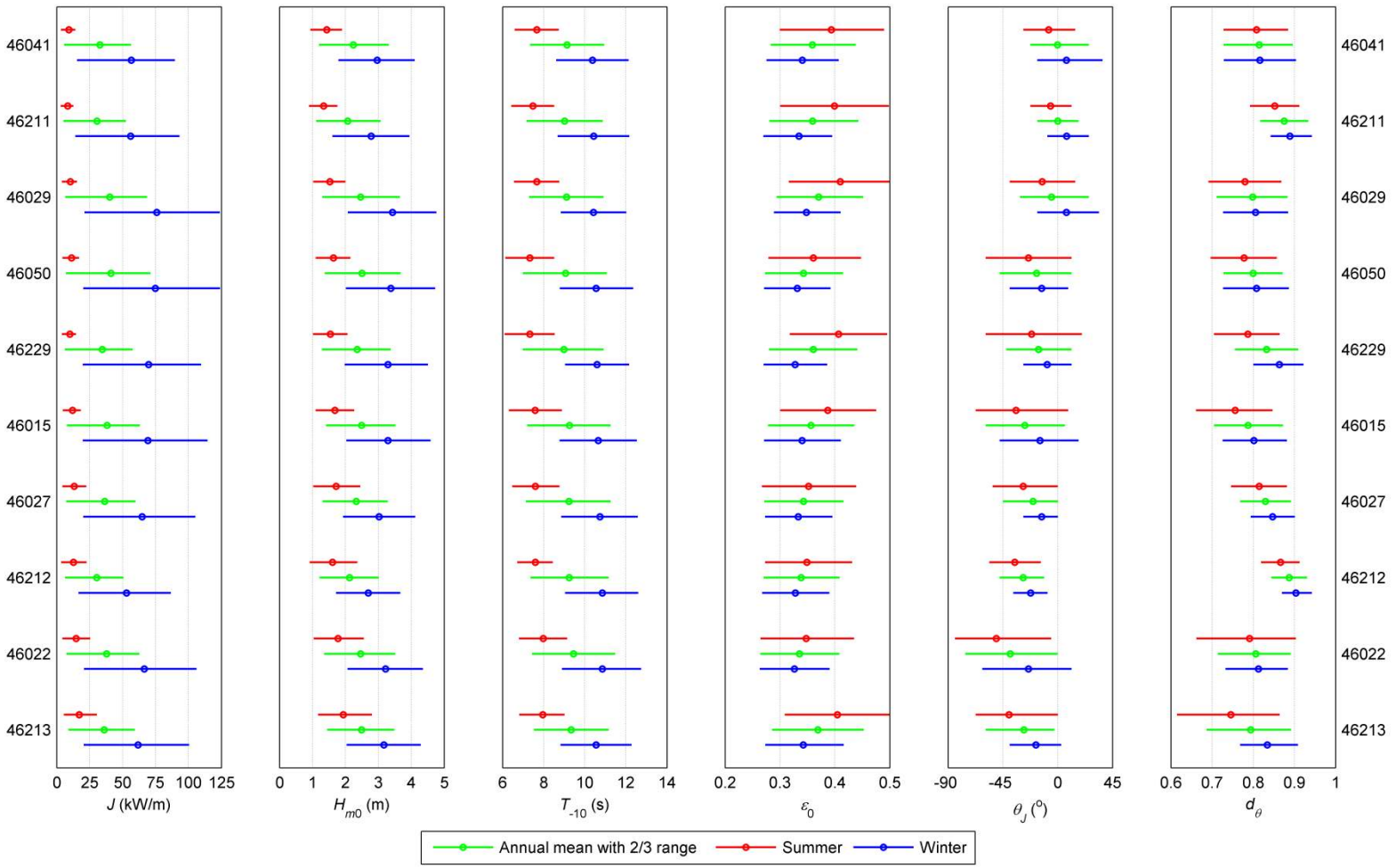

Figure 22. Mean value and 2/3 range (from 1/6 to 5/6 quantiles). Over full year, summer months and winter months for 6 characteristic quantities: wave power, J, significant wave height, H_{m0}, energy period, T_{-10}, spectral width, ϵ_0, direction of maximum directionally resolved power, θ_J and directionality coefficient, d_θ. Station ID numbers are ordered by latitude, with northernmost station at top.

As the stations in Figure 22 are ordered from north to south (e.g. station 46041 being the northernmost), some trends based on latitude may be seen. Most notably, the direction of maximum directionally resolved power is positively correlated with latitude ($R^2 = 0.88$), indicating that less of the incident wave power arrives from the north and northwest sectors for the stations that are located further north. Furthermore we see that during the summer months, when more energy arrives from the north, there is a negative correlation between latitude and both wave power ($R^2 = 0.78$) and significant wave height ($R^2 = 0.74$). It may be that Vancouver Island, the tip of which is visible at the top of Figure 18, is sheltering the northern buoys from the effects of waves from the north.

Significant interannual variability in the wave resource was observed. The mean wave power for winter seasons beginning in 1996 to 2007 is shown for several buoy locations in Figure 23. Where records are available for at least 10% of the clock hours and for at least two of the three winter months, a mean winter wave power is

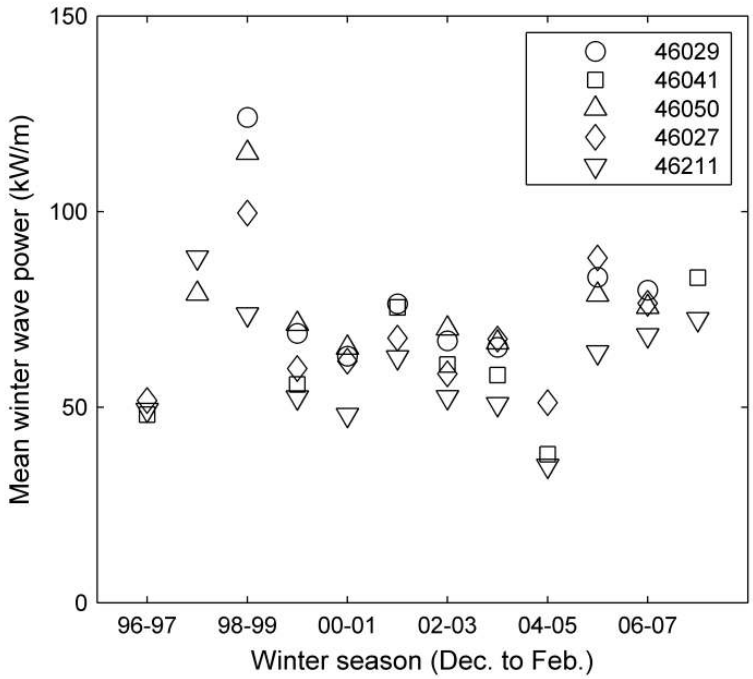

Figure 23. Mean winter wave power. For the winters of Dec. 1996 – Feb. 1997 through Dec. 2007 – Feb. 2008, at five wave measurement stations.

given. Note that while the wave power varies quite a bit from year to year (by a factor of 2 in some cases), the same general trend is followed by all 5 buoys.

5.2 Depth trends

A transformation of energy flux is expected as wave components travel over the continental shelf and are subject to refraction, bottom friction and, for obliquely arriving systems, sheltering by the coastline. Depending on the bathymetry, the effect of refraction can be a focusing or a diffusing of wave power. The coarse spatial distribution of the data buoys, however, along with significant gaps in the records, render comparisons between locations difficult. Although records have been weighted to avoid bias for or against any individual months, the interannual variability is significant. If a number of particularly stormy (or calm) events are missing from a given set of records, this may lead to bias in the assessment of the overall energy resource. That being said, it is certainly worthwhile to explore the implications of these records. Three buoys (i.e. 46027, 46211 and 46212) are located in depths between 40 and 50 m, and within 15 km of the shore, where wave components with periods as low as 8 s begins to feel the bottom. Stations 46211 and 46212 are the least energetic of the study, with mean annual wave power levels of 31 and 30 kW/m, respectively. However, with a mean annual wave power of 36 kW/m, station 46027 exhibits a gross power level similar to the deeper water locations, possibly due to a focusing effect of the underlying bathymetry. Quite clearly there is a greater directionality coefficient evident at the three relatively shallow locations, along with a decrease in the range of directions exhibited.

To get a closer look at the wave energy climate, we now focus on two stations with relatively long and complete records. Station 46029, located 40 km west of the mouth of the Columbia river at a mean depth of 135 m will be taken as representative of a relatively deep water site. Station 46211, located slightly further north at a mean depth of 40 m and 9 km from shore will be taken as representative of a shallower

location. A location of this depth and proximity to shore is more representative of sites at which offshore WECs may be installed in the near future.

5.3 Monthly statistics

To examine how the energy transport tends to change throughout the year, monthly statistics are presented for stations 46029 and 46211 in Figure 24 and Figure 25, respectively. For each of the characteristic quantities under investigation, a monthly mean as well as statistical ranges of observed values are presented. The seasonal trends discussed above are very clearly evidenced in these figures. Also evident in these monthly statistics are striking differences between the mean values and those that are exceeded 2.5% of the time. There is no need to design a WEC that can harvest a large proportion of the energy resource 100% of the time; indeed, this may not be possible technically or desirable economically [20]. On the other hand, these relatively infrequent, yet extreme, conditions pose a very real threat to the reliability and survivability of any practical device. While on average station 46211 experiences just over 3/4 the omnidirectional wave power of station 46029, the extreme values are similarly reduced. In the month of December, 97.5% of the time the significant wave height at station 46211 is below approximately 6 m and the wave power is below 250 kW/m. At station 46029, for the same percentage of time the maximum observed significant wave height and wave power are nearly 7.5 m and 340 kW/m, respectively. There may be no return on the added costs associated with a WEC designed to survive the relatively extreme climate of station 46029 (compared to 46211), especially when considering that the device may begin generating at rated capacity well before these 97.5% conditions. Additionally, the seas are directionally more uniform at station 46211. The mean directionality coefficient is 0.80 at the deeper station 46029, increasing to 0.88 at station 46211. Two-thirds of the time, the direction of maximum directionally resolved wave power occurs within a range of approximately 55° and 35° for stations 46029 and 46211, respectively.

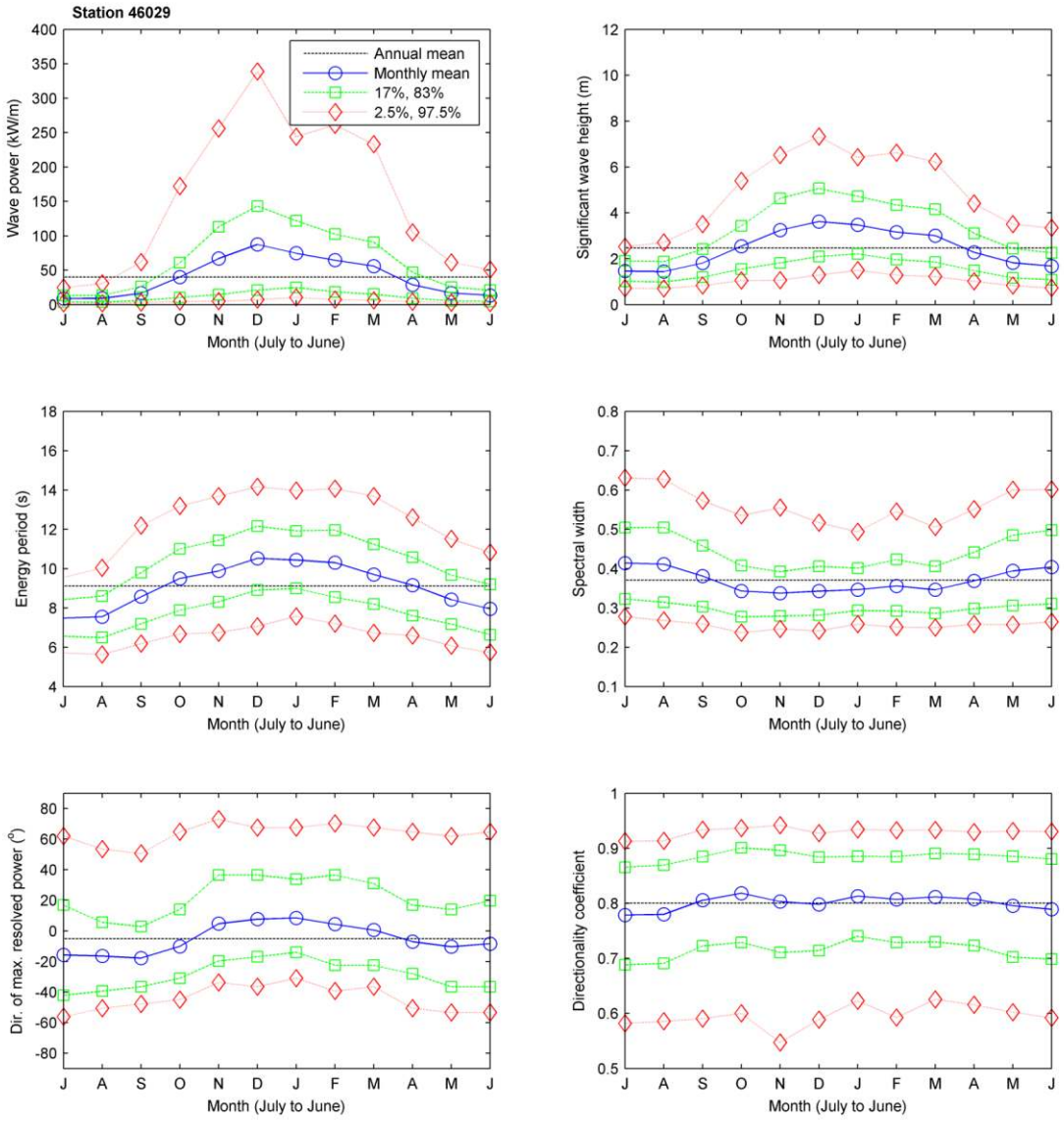

Figure 24. Monthly mean characteristic quantities, and statistical ranges, for station 46029.

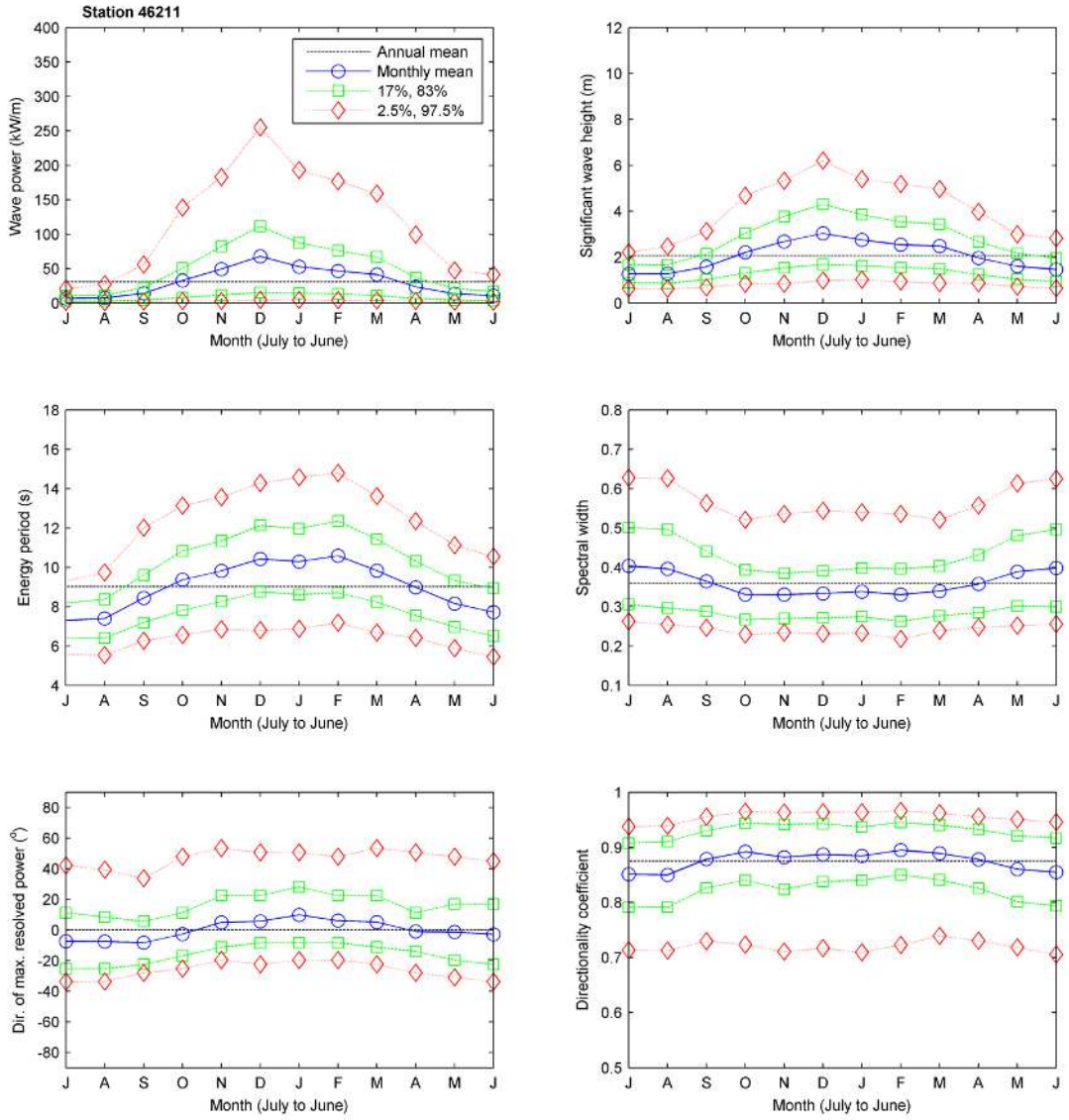

Figure 25. Monthly mean characteristic quantities, and statistical ranges, for station 46211.

Monthly means, along with statistical ranges, only begin to show the variability of wave climate that is hidden within an annual mean. Figure 26 illustrates the hourly variability of the characteristic quantities for station 46211 over a period of 1 year which, while typical in variability, shows no appreciable data gaps. Note, in particular, the sudden and drastic increases in wave power and significant wave heights.

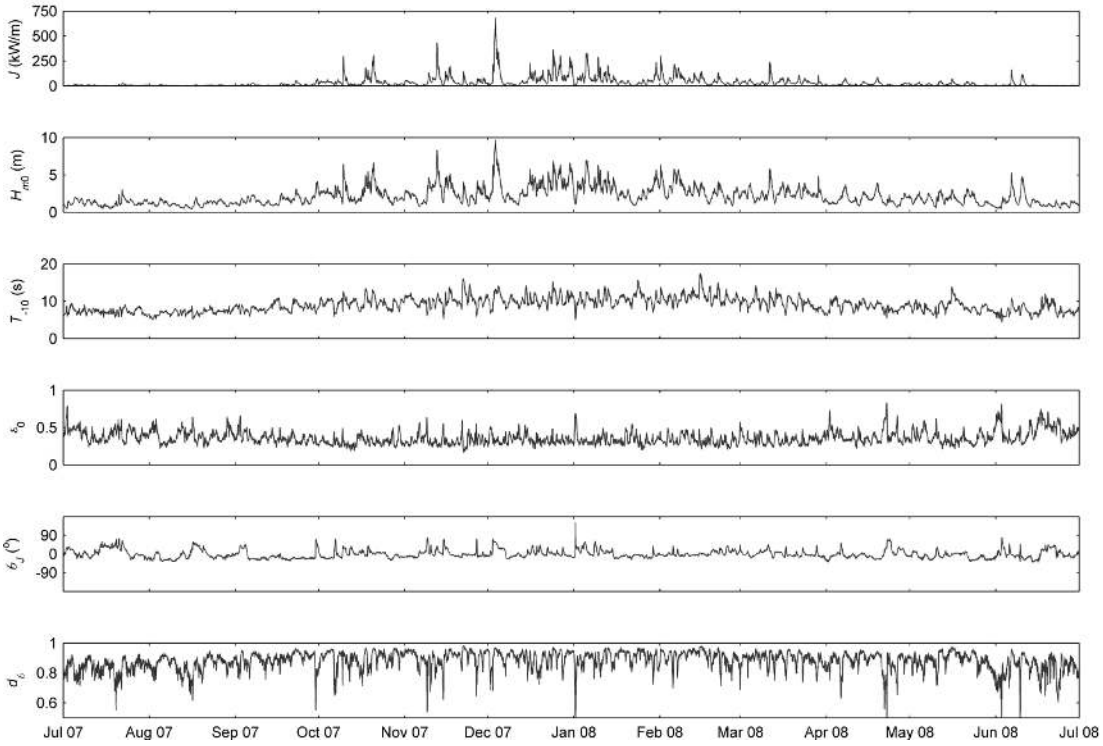

Figure 26. Hourly time series for six characteristic quantities at station 46211. The quantities are wave power, J, significant wave height, H_{m0}, energy period, T_{-10}, spectral width, ϵ_0, direction of maximum directionally resolved power, θ_J, and directionality coefficient, d_θ.

5.4 Distributions of occurrence and energy

While it is certainly necessary to understand how the characteristics of the wave resource are distributed over time, it is also crucial to consider distributions over energy. Figure 27 illustrates the empirical cumulative distributions of both occurrence and energy contribution, over six characteristic quantities. For station 46211 we see that wave power in excess of 200 kW/m occurs approximately 1% of the time, but accounts for 10% of the total energy. Also at station 46211, wave power is less than 10 kW/m for 40% of the time, while accounting for a mere 7% of the total energy. It

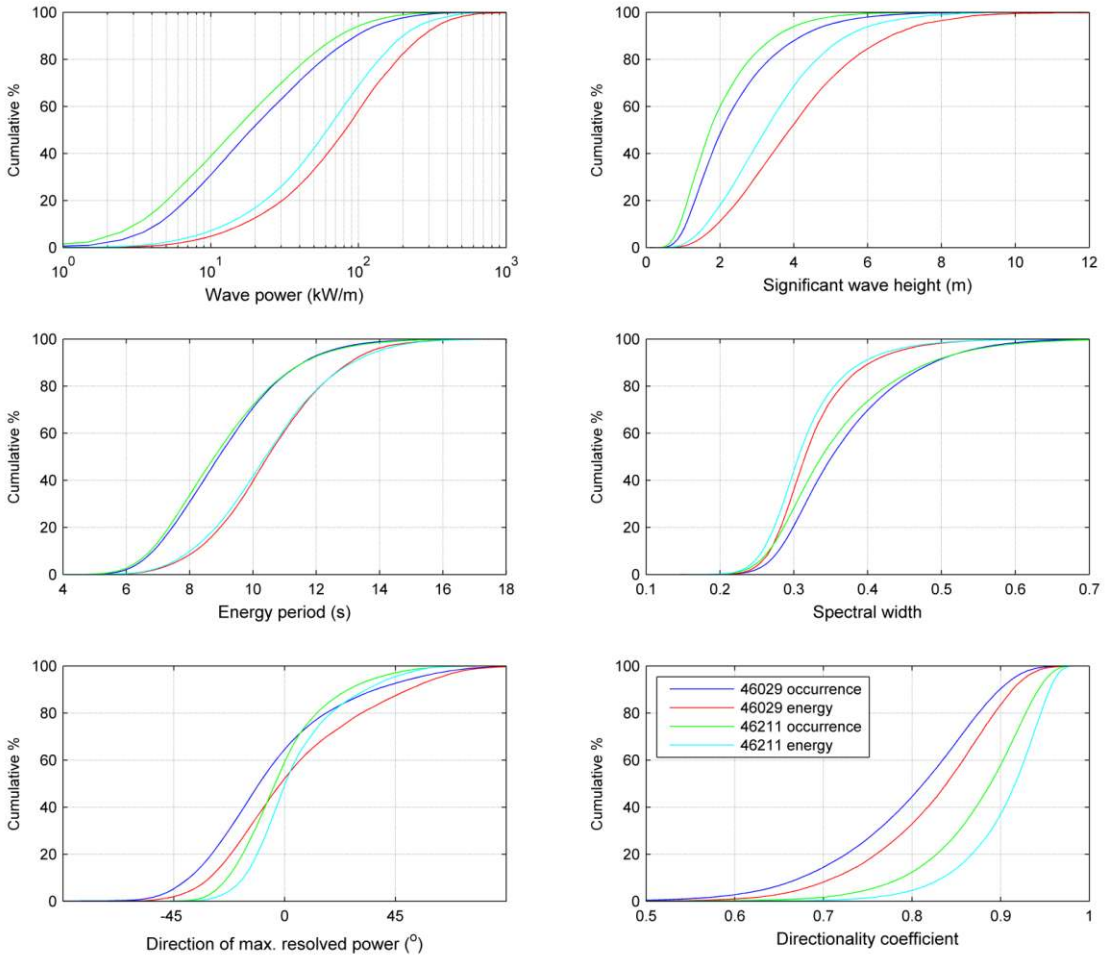

Figure 27. Empirical cumulative distributions of both total occurrence and total energy, for stations 46029 and 46211.

would seem that very little power is available for conversion for a large portion of the year. Additionally, a significant amount of energy arrives in conditions where, due to finite WEC generating capacity, only a small fraction of the resource can be converted.

Some WECs may be designed to operate in a survivability mode (e.g. locking up relative motion or submerging) during extreme conditions. If we arbitrarily assume a significant wave height of 6 m as a survivability mode threshold, 16% and 7% of the incident wave power would be entirely unavailable at stations 46029 and 46211, respectively.

There is little difference evident between the deeper and shallower water stations as far as energy period and spectral width are concerned. Sea states where the variance is distributed over a very wide range of frequencies (i.e. large spectral width) are observed to contribute relatively little to the incident energy. A spectral width greater than 0.4 occurs approximately 30% of the time, but contributes only 10% of the total energy. Considering the direction of maximum wave power, it is evident that at the shallower site, station 46211, the cumulative distributions of occurrence and energy are significantly narrower than those of the deeper site, station 46029. This indicates that the energy arrives within a narrower range of directions at the shallower site. It is also clear that the seas at station 46211 are much more uniform directionally. Sea states with a directionality coefficient of 0.9 or greater account for 62% of the energy at station 46211, and only 16% of the energy at station 46029.

5.5 Bivariate distributions

Scatter tables are often used to convey the frequency of occurrence of sea states defined by a characteristic wave height and period. Figure 28 presents, for stations 46029 and 46211, both the number of hours as well as the proportion of annual incident energy expected in an average year from sea states defined by H_{m0} and T_{-10}. Significant wave height is divided into bins of 0.5 m over a range of 0 to 10 m, with one more row for any sea states where H_{m0} is greater than 10 m.

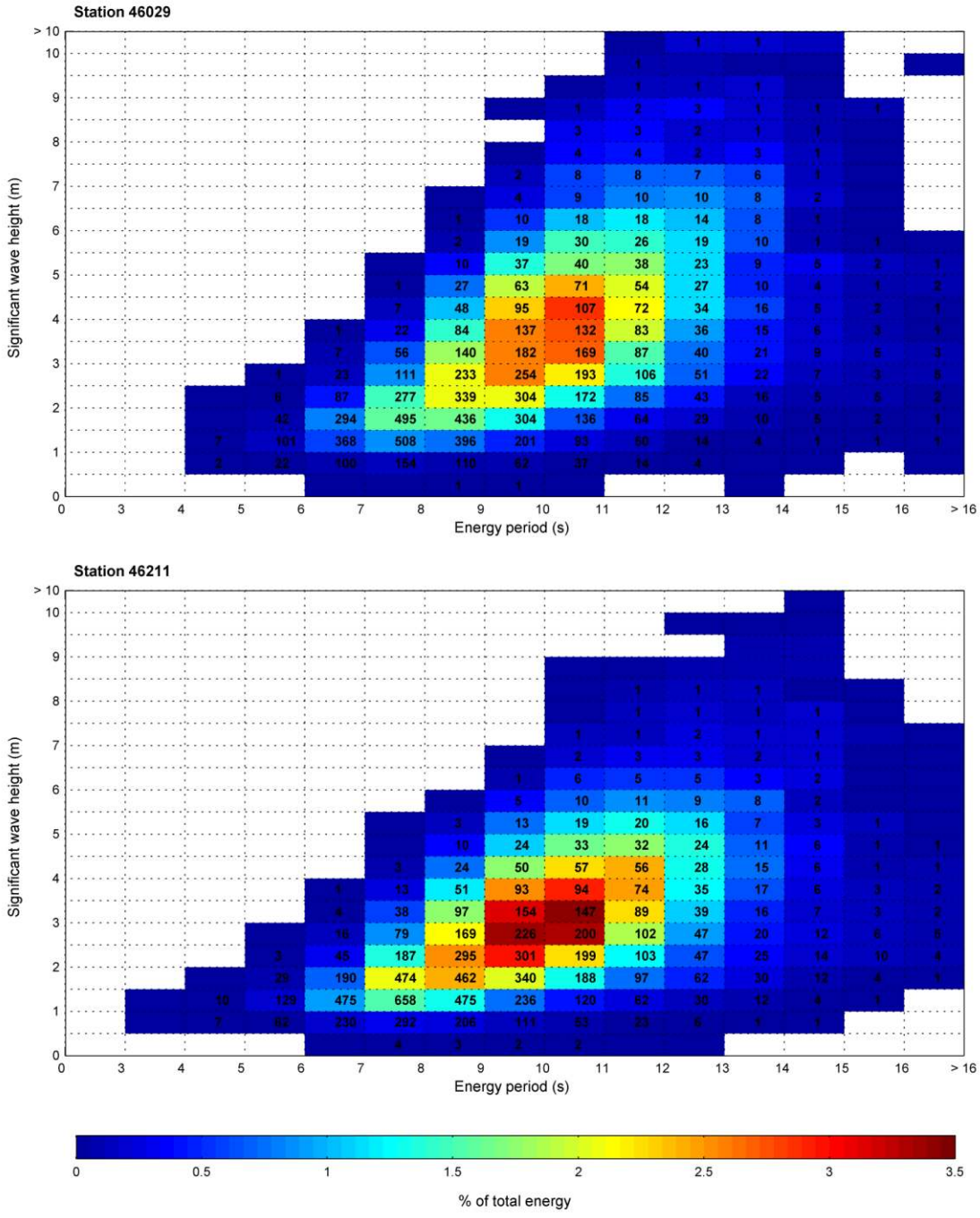

Figure 28. Bivariate distributions of occurrence and energy, for sea states defined by significant wave height and energy period, at stations 46029 and 46211. The color scale is used to represent the contribution of the sea state to the total incident energy, as a percentage, while the number indicates the annual hours of occurrence for an average year.

Similarly, the energy period is divided into bins of 1 s width over the range of 2 to 16 s. There is an additional column for sea states with an energy period greater than 16 s.

It is immediately clear upon examination of these combined scatter tables that sea states with the greatest rate of occurrence are not the same as those with the greatest energy. When evaluating risk of failure due to factors such as fatigue, wear or extreme loading scenarios the frequency of occurrence of each sea state will be of the utmost importance. When considering the degree to which power output can be delivered smoothly over time (on a scale of hours), occurrence is also important. The sea states with the greatest significant wave heights (e.g. H_{m0} > 7 m) do not contribute much to the total energy of the site, as they are expected to occur, at most, for only a few hours annually. However, consideration of these sea states is crucial to an analysis of reliability and survivability. Sea states with the greatest frequency of occurrence (e.g. 400 or more hours annually) contribute somewhat more to the total energy, but due to their lower significant wave heights and energy periods their contribution to total annual energy does not match their contribution to time. The sea states with the greatest contribution to energy, appearing in orange and red, have significant wave heights between 2 and 5 m and energy periods between 8 and 12 s. Note that at station 46211 the peak of the energy distribution is higher and falls away faster than that of station 46029, as evidenced by the dark red giving way quickly to cooler colors in the scatter table of station 46211. This is indicative of a greater concentration of the annually available energy resource, within a smaller range of sea states.

5.6 Weather windows

Whether one is considering a single device or a large array of WECs, long term operation is certain to entail these three things: deployment, maintenance and retrieval. While routine maintenance might well be performed in place, major maintenance or repair could involve the retrieval and subsequent redeployment of a device. Although

the specifics will depend on the WEC, the service vessel and the required actions, there will be times when conditions allow for these operations, and times when conditions preclude them. A detailed discussion of operational effectiveness can be found in Lloyd [59].

On the assumption that if the significant wave height remains below some threshold for at least an operationally-dependant length of time, a general view of the likelihood of being able to perform a given operation can be had by examining weather windows. Expectation of various weather windows are presented in Figure 29 and Figure 30 for stations 46029 and 46211, respectively. The percentage of time in which the significant wave height remains below a given value for at least a given amount of time is shown on an annual basis, as well as for each of the four seasons.

Previously discussed analysis in this study used a method of weighting to account for the bias introduced by gaps in the records (see Section 3.3). Because the significant wave height records must be examined as a time series for these persistence statistics, the data was handled in a different manner for this portion of the study. Gaps of less than a certain length were filled in using the method of "folding-in" [27]. With this method the first half of each gap is filled in with the previous data sequence, but in a reverse order. The second half of the gap is filled in with the following data sequence, again in a reverse order. In this study a threshold of 12 hours was used, to reduce the likelihood of filling in completely missing storms with data from surrounding periods of calm. After filling in the numerous small gaps, a number of gapless segments (typically 2 to 12) remained, separated by gaps of 12 hours or more. It was now possible to determine the total number of hours in which the significant wave height remained below a given threshold for at least a given number of hours, without the hundreds of small gaps "breaking up" the windows. Windows that occurred across more than one season (e.g. beginning in spring and ending in summer) were considered as weather windows of the entire length of persistence, with the observed number of hours occurring in each season assigned to that season. In calculating percent occurrence, only those hours with records were considered.

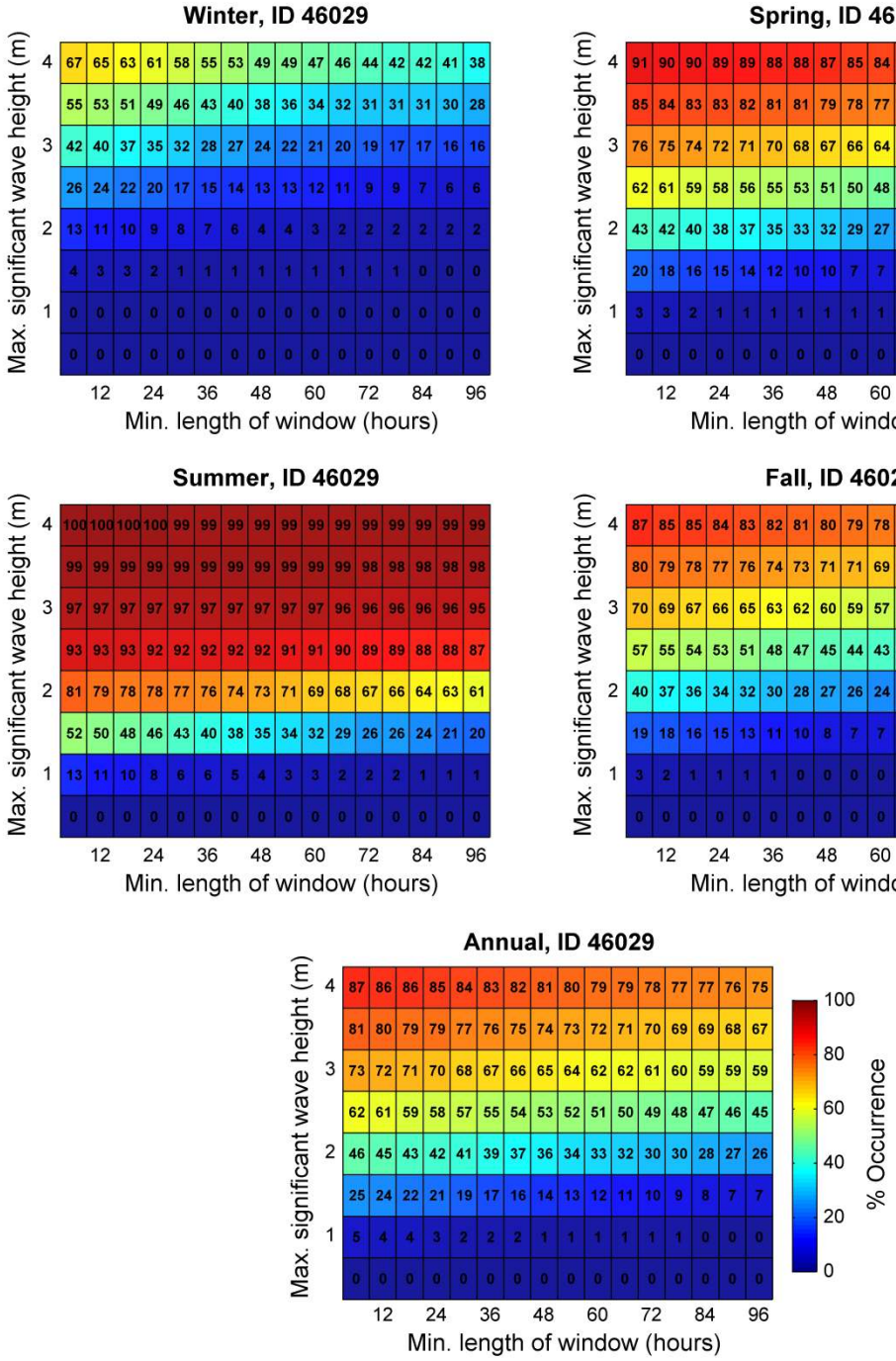

Figure 29. Expectation of weather windows for station 46029. Depicted for each season, and on an annual basis, is the percent of time in which the significant wave height remains below a given value, continuously, for at least a given number of hours.

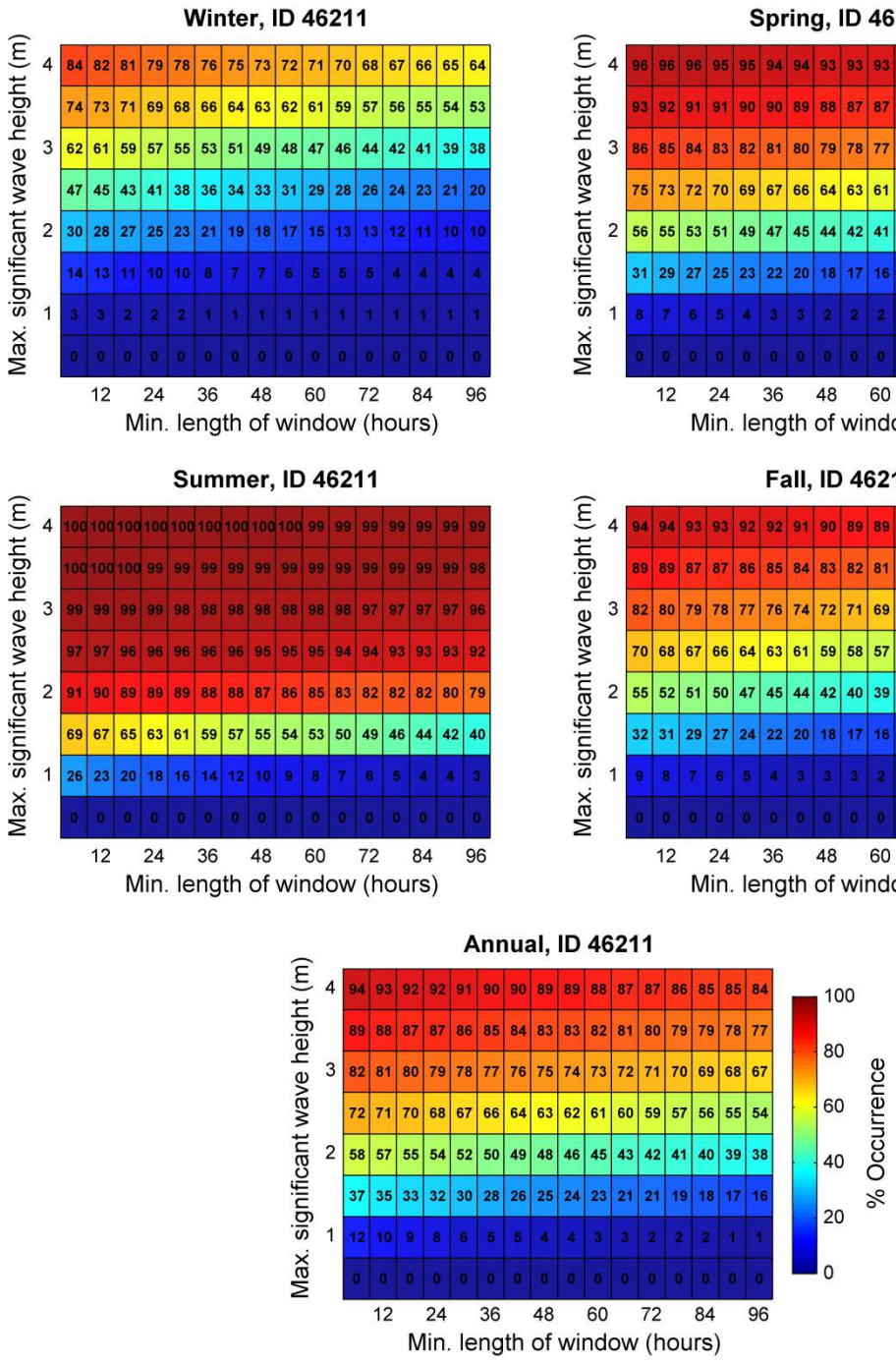

Figure 30. Expectation of weather windows for station 46211. Depicted for each season, and on an annual basis, is the percent of time in which the significant wave height remains below a given value, continuously, for at least a given number of hours.

Examining the expectations of weather windows in Figure 29 and Figure 30, it is clear that opportunities for deployment, retrieval or maintenance occur more frequently at station 46211 than station 46029. We have shown that wave heights tend to be lower at 46211 (see e.g. Figure 24 and Figure 25), so this is as expected. At either location, and presumably at any location, if the time necessary to perform an operation can be reduced, the expectation of a suitable weather window increases. The occurrence of weather windows is much greater in the summer than in the winter, with spring and fall lying somewhere in between. By way of example, for station 46211 the percent of time in which the significant wave height remains below 2 m for at least 72 hours is 13%, 37%, 82%, and 35% for winter, spring, summer and fall, respectively. Thus, planned maintenance may best be scheduled in the summer months. Additionally, when considering the possibility of device failure it must be understood that the seasonally occurring storms that threaten WECs will also limit repair and retrieval operations.

5.7 Representative spectra

Estimations of WEC response (e.g. power performance or operational loads) to a diverse range of sea states must be determined if the various distributions presented in Sections 5.1-5 are to inform decision making in designing and siting. While measurement of full scale devices at sea may provide the best data, this is not practical for most stages of design, and so physical and computational modeling will be necessary. Simulations of hourly sea states over even a single year's time (8760 in all) would be prohibitive, for all but the simplest models. If, however, a limited number of spectra could be used to represent the expected sea states, then this comprehensive modeling is feasible.

An algorithm was developed for this study which synthesizes a set of representative frequency variance spectra for a given location, given the archived spectra as input. The sea states were divided into bins, similar to the bivariate distributions discussed in Section 5.5. However, in this case a trivariate division was

implemented, using significant wave height, energy period and spectral width. A weighted-averaging of all spectra in a bin, using the weights discussed in Section 3.3, yielded a spectrum representative of the conditions defining the bin. Bin widths of 1 m and 1 s were used for significant wave height and energy period, with all spectra of $T_{-10} > 16$ s included in one bin. Three spectral width bins of width 0.1 between 0.2 and 0.5, with a two additional bins: one for spectra where $\epsilon_0 < 0.2$, and another for spectra where $\epsilon_0 > 0.5$. These divisions are arbitrary, but were chosen to limit the number of representative spectra, while preserving some distinctions between disparate sea states. As characteristic quantities of directionality were not considered in this case, the resulting spectra may be best suited to a single, axisymmetric device. If deemed necessary, a similar strategy could be implemented using any number of characteristic quantities. Keep in mind, however, that increasing the number of parameters would naturally increase the number of representative sea states.

The expected frequency of occurrence and contribution to total energy of each representative spectrum was easily calculated, as each individual spectrum's weight (see Section 3.3) is equal to the number of hours in which it is expected to occur over a time equal to the length of the analyzed record. The weighted-average spectrum of a given trivariate sea state was included in the representative set if, and only if, it met any one of the following three criteria:

1. contribution of at least 0.1% to total energy,
2. expected frequency of occurrence of at least 0.2%, or
3. significant wave height of at least 7 m.

These three criteria insure that conditions relevant to power performance, fatigue loading and extreme loading are represented.

Frequency variance spectra representative of the wave resource at station 46211 (see Tables 1 and 2 for location, depth, etc.) are presented in the appendix. Using the methodology and criteria presented in the preceding paragraphs, approximately 129,000 spectra recorded between 1987 and 2008, were reduced to a representative set of 159 spectra. This limited set of sea states accounts for 97% of

total energy and 97% of total occurrence at station 46211. A total of 123 spectra met the 1st criterion, accounting for 95% of the total energy and 86% of all occurrences. If one was interested only in power production, these spectra would be sufficient. Seventeen sea states met only the 2nd criterion, and accounted for 1.1% of the total energy and 10% of occurrences. Although their contribution to energy may be negligible, with an expected occurrence of 10% they should be accounted for when evaluating long-term issues, such as wear and fatigue. Nineteen sea states met only the 3rd criterion, accounting for 0.9% of total energy and 0.06% of occurrences. With significant wave heights in excess of 7 m, it will be important to consider these sea states in survivability studies.

Local bathymetric effects will produce spatial variability in the resource, particularly so in depths where WECs are likely to be installed in the near future (e.g. $\geq$50 m). Even though conditions may not be identical at other locations of similar depth, station 46211 is a good candidate for the representation of offshore WEC deployment sites in the US Pacific Northwest. Spectral records over a span of 22 years were available for this study, lending statistical significance to the results, and the buoy is located at a depth and distance to shore (i.e. 40 m and 9 km) similar to those proposed. Though not included in this publication, a set of representative spectra was also generated for station 46029. Although this location may be deeper and further to sea than WECs are likely to be deployed in the near future, the representative spectra may be numerically propagated into specific locations using e.g. SWAN.

6. CONCLUSION

6.1 Conclusion

The wave energy resource has been assessed and characterized at 10 locations in the US Pacific Northwest using archived spectral records from wave measurement buoys. Bias due to missing records was compensated for by weighting the existing records such that the appropriate number of hours for each month was considered. The wave energy resource at each location was characterized using six quantities derived from each individual hourly spectrum: omnidirectional wave power, significant wave height, energy period, spectral width, direction of maximum directionally resolved wave power and directionality coefficient. Because any given WEC must both convert this energy and survive the environment, the qualities of energy transport are especially important.

It was shown that at any given location the variability of sea states defined by these characteristic quantities is considerable, and should be accounted for when designing and siting ocean wave energy converters. Strong seasonal trends were observed, with greater wave power, significant wave height, energy period and directionality coefficient, and narrower spectral width, when comparing winter months to summer months. The mean wave power during the winter months was found to be up to 7 times that of the summer mean. The direction of maximum directionally resolved wave power tends to head more towards the south in the summer months, with θ_J typically 10° to 20° less in the summer than in the winter. The sea states observed at stations closer to shore (depth < 50m) exhibited much greater directional uniformity, with a larger directionality coefficient and the direction of maximum directionally resolved wave power occurring within a smaller range. Interannual variability is also considerable, with the maximum and minimum mean annual winter wave powers differing by up to a factor of two at some stations.

The wave resource was presented in detail for two representative locations, with mean water depths of 135 and 40 m. Monthly means and statistical ranges were

presented for the six characteristic quantities, showing the broad range of sea states that should be anticipated at any time of the year. In addition to knowing how the characteristics of the wave resource are distributed over time, it is critical to consider distributions over energy. Empirical cumulative distributions were presented, in terms of both occurrence and contribution to total energy, for six quantities characterizing the resource. While a mean annual wave power of 31 kW/m was observed at the shallower location (i.e. station 46211), mean hourly wave power varied over a vast range. Wave power of 10 kW/m or less occurs 40% of the time, contributing only 8% of the expected annual energy while wave power of 200 kW/m or more occurs 1% of the time and accounts for 10% of the annual energy.

Combined scatter tables show the expected hours of occurrence and contribution to annual energy for sea states defined by significant wave height and energy period. The sea states that contribute most to the annual energy have significant wave heights between 2 and 5 m and energy periods between 8 and 12 s. Sea states below these ranges may be very common, but the associated wave power is so low that little contribution is made to the total annual energy. The sea states with the greatest significant wave heights, while very powerful, do not contribute greatly to the total annual energy due to a very low expectation of occurrence. However, consideration of these sea states is critical to the survivability and reliability of a WEC.

Expectation of weather windows were tabulated on an annual basis, as well as for each of four seasons. As expected, the likelihood of significant wave height remaining below an operationally dependant threshold for at least a given length of time is highly seasonal. It would appear that planned maintenance may best be scheduled in the summer months.

Physical and computational modeling will be necessary to estimate WEC response (e.g. power performance, fatigue analysis, extreme loading) to the diverse range of expected sea states. A limited number of representative frequency variance spectra, along with expected frequency of occurrence and contribution to total energy,

are presented as modeling input. These spectra represent 97% of total energy and 97% of total occurrence at station 46211, and all sea states with a significant wave height in excess of 7 m.

6.2 Recommendations for future work

The resource characterization resulting from the present work is spatially coarse. A more refined assessment at locations of particular interest would be the logical next step. The frequency-directional spectra from an appropriate station could be propagated numerically using e.g. SWAN. Analysis would ideally be performed at a number of spatial grid points within the area of interest, allowing for an assessment of the local bathymetric affects.

It would be useful to validate the representative spectra. A hydrodynamic model, developed to predict e.g. power performance or operational stresses, could be implemented using a number of individual spectra from a given bin, as well as the weighted-average representative spectra, and the results compared. It is quite plausible that the bin widths could be increased, reducing the necessary number of representative spectra. It is also plausible that one or more bin widths need to be reduced, for a sufficiently accurate representation. Additionally, different WECs may be sensitive to different characteristic quantities. As an example, spectral width may be irrelevant, and directional width necessary, for some WEC morphologies. Along these lines, correlating the performance (or critical stresses) of prototypes or full-scale devices with the various characteristic quantities would be immensely useful. Unfortunately, though understandably, this data is often proprietary.

BIBLIOGRAPHY

[1] N.N. Panicker, Power resource estimate of ocean surface waves, Ocean Engineering. 3 (1976) 429–434.

[2] J. Cruz, ed., Ocean wave energy, Berlin Heidelberg, Springer-Verlag, 2008.

[3] Energy Information Administration, International energy outlook, available at www.eia.doe.gov/oiaf/ieo/index.html, accessed March, 2009.

[4] A. Clément, P. McCullen, A. Falcão, A. Fiorentino, F. Gardner, K. Hammarlund, et al., Wave energy in Europe: current status and perspectives, Renewable and Sustainable Energy Reviews. 6 (2002) 405-431.

[5] B. Drew, A.R. Plummer, M.N. Sahinkaya, A review of wave energy converter technology, Proceedings of the Institution of Mechanical Engineers, Part A: Journal of Power and Energy. 223 (2009) 887-902.

[6] Wave Dragon, http://www.wavedragon.net, accessed May, 2010.

[7] Oceanlinx, http://www.oceanlinx.com, accessed May, 2010.

[8] Voith Hydro Wavegen Limited, http://www.wavegen.co.uk, accessed May, 2010.

[9] LIMPET, http://tinyurl.com/LIMPET-OWC, accessed April, 2010.

[10] Pelamis Wave Power, http://www.pelamiswave.com, accessed May, 2010.

[11] Aquamarine Power Oyster, http://tinyurl.com/Aquamarine-Oyster, accessed April, 2010.

[12] Columbia Power Technologies WEC, http://tinyurl.com/CPT-OWEC, accessed May, 2010.

[13] Ocean Power Technologies, http://www.oceanpowertechnologies.com, accessed April, 2010.

[14] Archimedes Wave Swing AWS, http://tinyurl.com/ArchimedesWaveSwing, accessed May, 2010.

[15] Aquamarine Power, http://www.aquamarinepower.com, accessed May, 2010.

[16] Columbia Power Technologies, http://www.columbiapwr.com, accessed April, 2010.

[17] AWS Ocean Energy, http://www.waveswing.com, accessed May, 2010.

[18] M. French, On the difficulty of inventing an economical sea wave energy converter: a personal view, Proceedings of the Institution of Mechanical Engineers, Part M: Journal of Engineering for the Maritime Environment. 220 (2006) 149-155.

[19] J. Falnes, Principles for Capture of Energy from Ocean Waves. Phase Control and Optimum Oscillation., Department of Physics, NTNU, N-7034 Trondheim, Norway. (1997).

[20] J. Falnes, Small is beautiful: How to make wave energy economic, in: 1993 European Wave Energy Symposium, Edinburgh, Scotland, 1994: pp. 367-372.

[21] J. Falnes, Ocean waves and oscillating systems, New York, Cambridge University Press, 2002.

[22] NOAA's National Weather Service, WAVEWATCH III™ Model, http://tinyurl.com/WaveWatchIII, accessed May, 2010.

[23] S. Hasselmann, K. Hasselmann, E. Bauer, P. Janssen, G.J. Komen, L. Bertotti, et al., The WAM model-a third generation ocean wave prediction model, Journal of Physical Oceanography. 18 (1988) 1775–1810.

[24] M.T. Pontes, Assessing the European wave energy resource, J. Offshore Mech. Arct. Eng. 120 (1998) 226-231.

[25] M.G. Hughes, A.D. Heap, National-scale wave energy resource assessment for Australia, Renewable Energy. 35 (2010) 1783-1791.

[26] A.M. Cornett, A global wave energy resource assessment, in: International Offshore and Polar Engineering Conference, Vancouver, Canada, 2008: pp. 318-323.

[27] M.J. Tucker, E.G. Pitt, Waves in ocean engineering, Oxford, Elsevier, 2001.

[28] APB Marine Environmental Research Ltd., Atlas of UK marine renewable energy resources: Technical Report, Report No. R.1432, 2008.

[29] D. Mollison, M.T. Pontes, Assessing the Portuguese wave-power resource, Energy. 17 (1992) 255–268.

[30] M.T. Pontes, R. Aguiar, H.O. Pires, A nearshore wave energy atlas for Portugal, J. Offshore Mech. Arct. Eng. 127 (2005) 249-255.

[31] R. Waters, J. Engström, J. Isberg, M. Leijon, Wave climate off the Swedish west coast, Renewable Energy. 34 (2009) 1600-1606.

[32] C. Beels, J. De Rouck, H. Verhaeghe, J. Geeraerts, G. Dumon, Wave energy on the Belgian Continental Shelf, in: OCEANS 2007-Europe, 2007: pp. 1–6.

[33] A.M. Cornett, Inventory of Canada's offshore wave energy resources, in: Proc. Offshore Mech. Arct. Eng., Hamburg, Germany, 2006.

[34] Z. Defne, K.A. Haas, H.M. Fritz, Wave power potential along the Atlantic coast of the southeastern USA, Renewable Energy. 34 (2009) 2197-2205.

[35] TU Delft - The official SWAN Home Page, http://www.swan.tudelft.nl, accessed April, 2010.

[36] G. Iglesias, M. López, R. Carballo, A. Castro, J. Fraguela, P. Frigaard, Wave energy potential in Galicia (NW Spain), Renewable Energy. 34 (2009) 2323-2333.

[37] G. Iglesias, R. Carballo, Wave energy resource in the Estaca de Bares area (Spain), Renewable Energy. 35 (2010) 1574-1584.

[38] J.H. Wilson, A. Beyene, California wave energy resource evaluation, Journal of Coastal Research. 23 (2007) 679–690.

[39] A. Beyene, J.H. Wilson, Comparison of wave energy flux for northern, central, and southern coast of California based on long-term statistical wave data, Energy. 31 (2006) 1520–1533.

[40] A. Beyene, J.H. Wilson, Digital mapping of California wave energy resource, International Journal of Energy Research. 31 (2007).

[41] Electric Power Research Institute, Survey and characterization of potential offshore wave energy sites in Oregon (2004), available at http://tinyurl.com/EPRI-Oregon, accessed March, 2010.

[42] Electric Power Research Institute, Survey and characterization of potential offshore wave energy sites in Washington (2004), available at http://tinyurl.com/EPRI-Washington, accessed March, 2010.

[43] R.G. Dean, R.A. Dalrymple, Water wave mechanics for engineers and scientists, Singapore, World Scientific, 1991.

[44] L.H. Holthuijsen, Waves in oceanic and coastal waters, New York, Cambridge University Press, 2007.

[45] I.R. Young, Wind generated ocean waves, Netherlands, Elsevier, 1999.

[46] M.K. Ochi, Ocean waves, Cambridge, Cambridge University Press, 1998.

[47] S.K. Chakrabarti, Hydrodynamics of offshore structures, Computational Mechanics, 1987.

[48] National Data Buoy Center, Nondirectional and directional wave data analysis procedures, NDBC Technical Document 96-01, 1996.

[49] National Data Buoy Center, Handbook of automated data quality control checks and procedures, NDBC Technical Document 96-02, 2009.

[50] Coastal Data Information Program Documentation, http://tinyurl.com/CDIP-documentation, accessed April, 2010.

[51] M. Benoit, P. Frigaard, H.A. Schaffer, Analysing multidirectional wave spectra: a tentative classification of available methods, in: Proc. Seminar on Multidirectional Waves and Their Interaction with Structures, 1997: pp. 131–158.

[52] H. Mitsuyasu, F. Tasai, T. Suhara, S. Mizuno, M. Ohkusu, T. Honda, et al., Observations of the directional spectrum of ocean waves using a cloverleaf buoy, Journal of Physical Oceanography. 5 (1975) 750–760.

[53] M.A. Kerbiriou, M. Prevosto, C. Maisondieu, A. Babarit, A. Clément, Influence of an improved sea-state description on a wave energy converter production, in: Proceedings of the 26th International Conference on Offshore Mechanics and Arctic Engineering, San Diego, California, 2007.

[54] M.S. Longuet-Higgins, Statistical properties of wave groups in a random sea state, Philosophical Transactions of the Royal Society of London. Series A, Mathematical and Physical Sciences. (1984) 219-250.

[55] D. Mollison, Wave climate and the wave power resource, in: Evans D.V., Falcao A.F.O., Ed., Hydrodynamics of Ocean Wave-Energy Utilization - IUTAM Syposium, Lisbon, 1985, Berlin, Heidelberg, Springer-Verlag, 1986: pp. 133–156.

[56] G.H. Smith, V. Venugopal, J. Fasham, Wave spectral bandwidth as a measure of available wave power, in: Proc. of Int. Conf. Offshore Mech. Arct. Eng., Hamburg, Germany, 2006: pp. 423-431.

[57] J.B. Saulnier, P. Ricci, M.T. Pontes, A.F. Falcao, Spectral bandwidth and WEC performance assessment, in: 7th European Wave and Tidal Energy Conference, Porto, Portugal, 2007.

[58] E.G. Pitt, Assessment of wave energy resource, European Marine Energy Centre, 2009.

[59] A.R.J.M. Lloyd, Seakeeping, Sussex, Ellis Horwood, 1989.

APPENDIX

Representative spectra for station 46211

Frequency variance spectra representative of the wave resource at station 46211 (see Tables 1 and 2) are presented in this appendix.. A total of 129,000 spectra, recorded between 1987 and 2008, were reduced to a representative set of 159, as described in Section 5.7. This limited set of spectra account for 97.2% of total energy and 96.8% of total occurrence at station 46211. The organization of the spectra is as follows. Firstly, by significant wave height in increments of 1 m, and secondly by energy period in increments of 1 s. Spectra representing different spectral widths are displayed together in the same plot. See Section 5.7 for details.

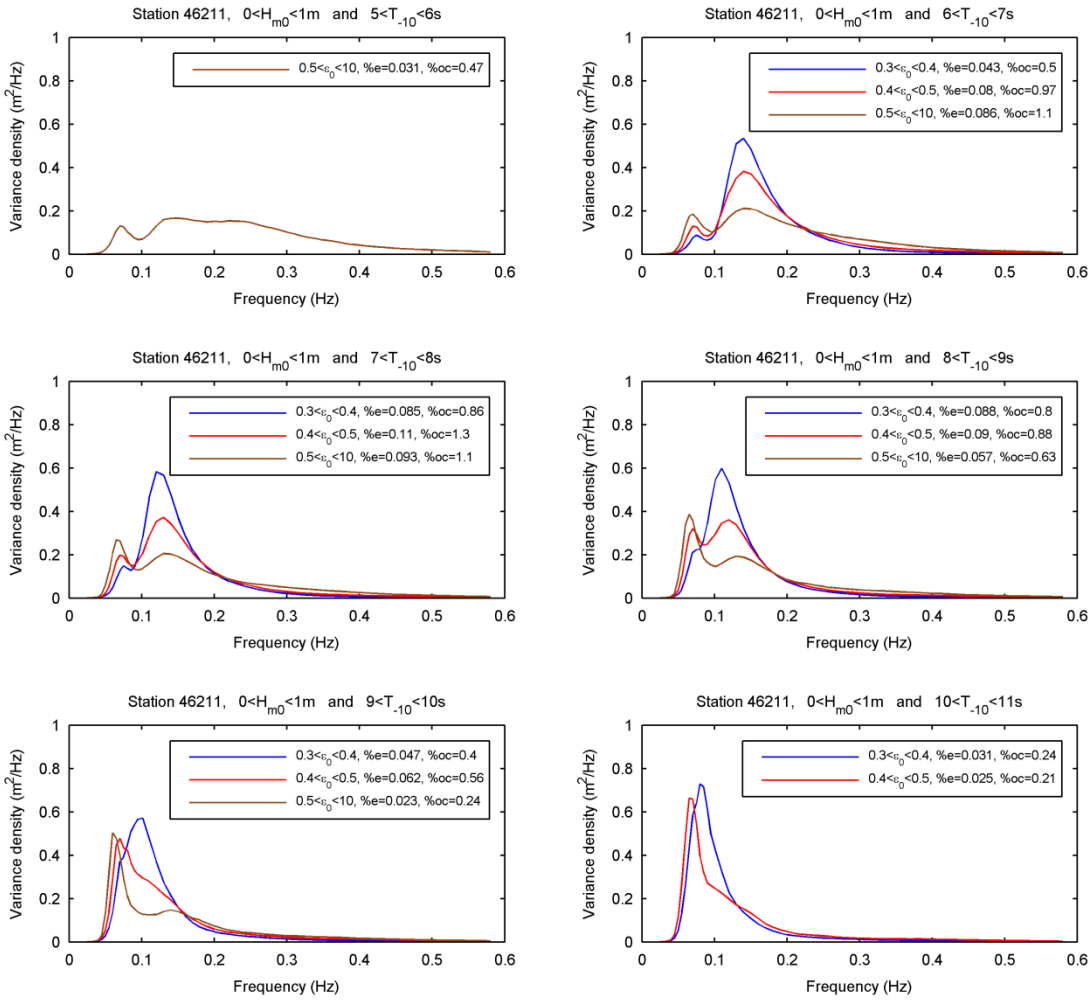

Figure A 1. Representative spectra for station 46211, $0<H_{m0}<1$ m.

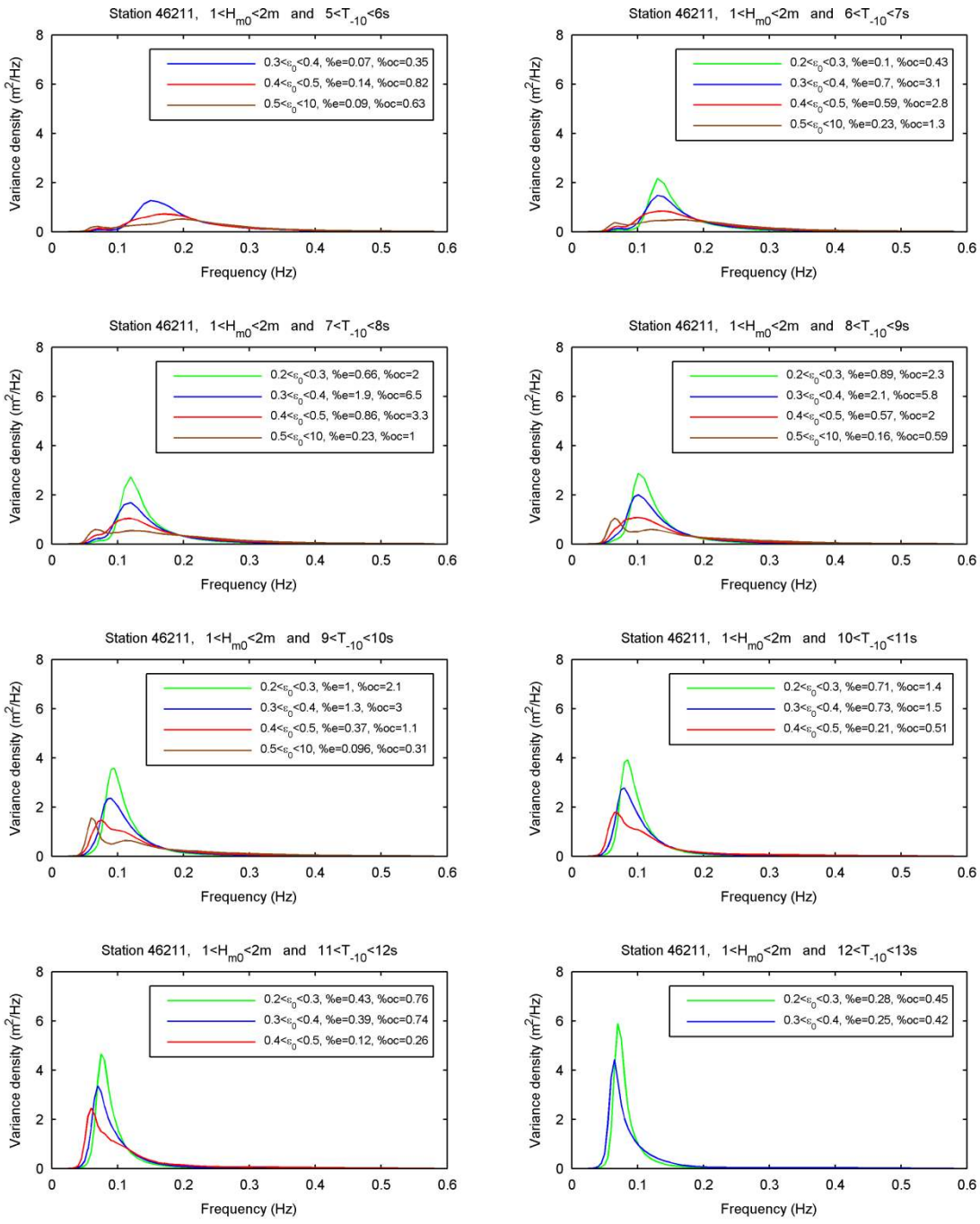

Figure A 2. Representative spectra for station 46211, 1<H_{m0}<2 m (1 of 2).

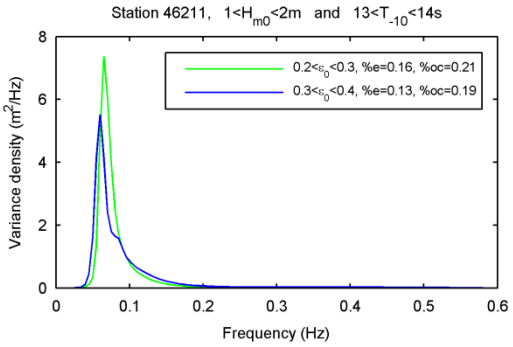

Figure A 3. Representative spectra for station 46211, 1<H_{m0}<2 m (2 of 2).

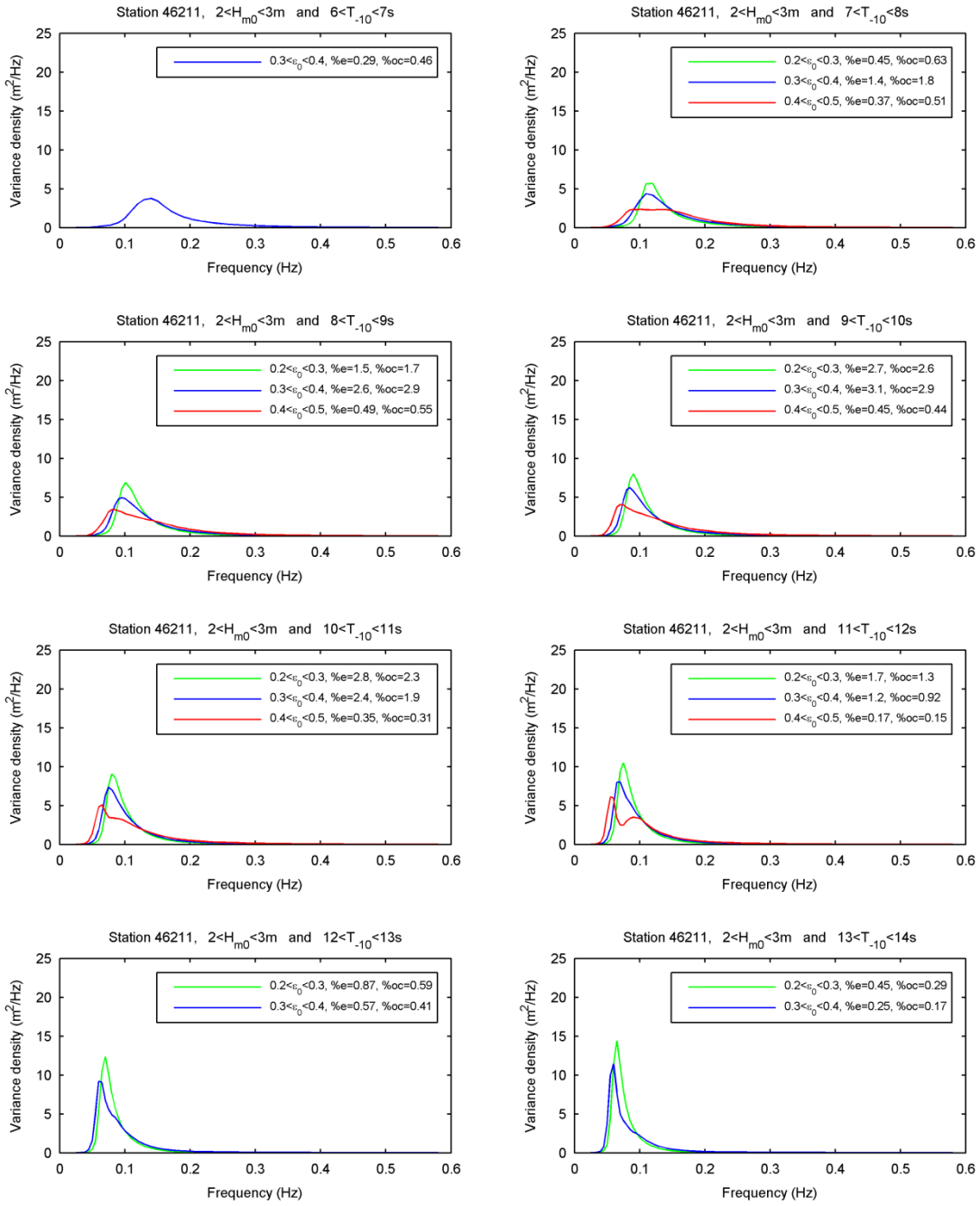

Figure A 4. Representative spectra for station 46211, 2<H_{m0}<3 m (1 of 2).

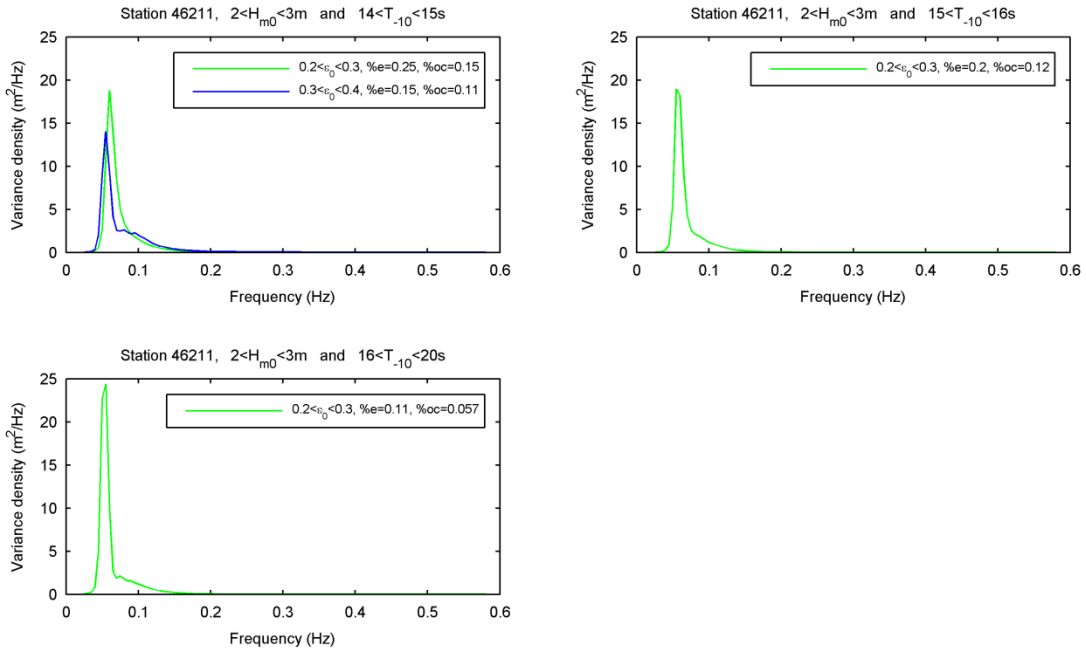

Figure A 5. Representative spectra for station 46211, 2<H_{m0}<3 m (2 of 2).

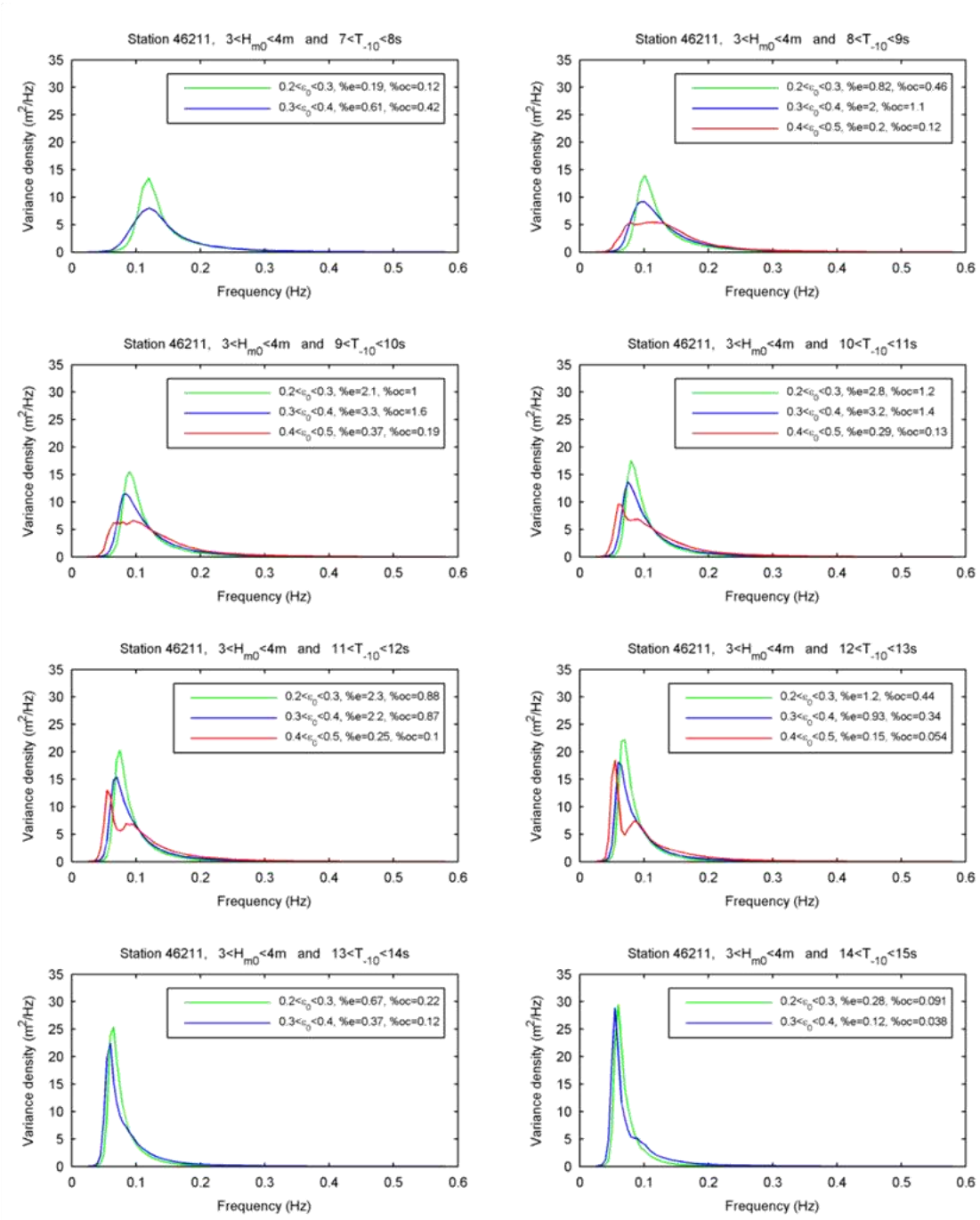

Figure A 6. Representative spectra for station 46211, 3<H_{m0}<4 m (1 of 2).

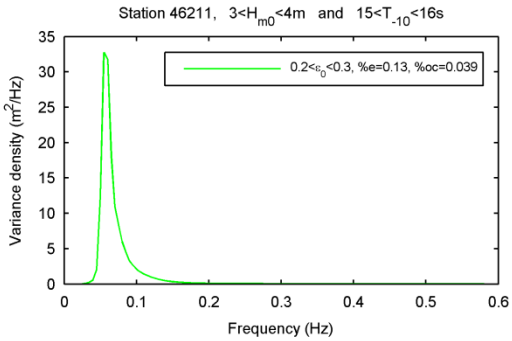

Figure A 7. Representative spectra for station 46211, 3<H_{m0}<4 m (2 of 2).

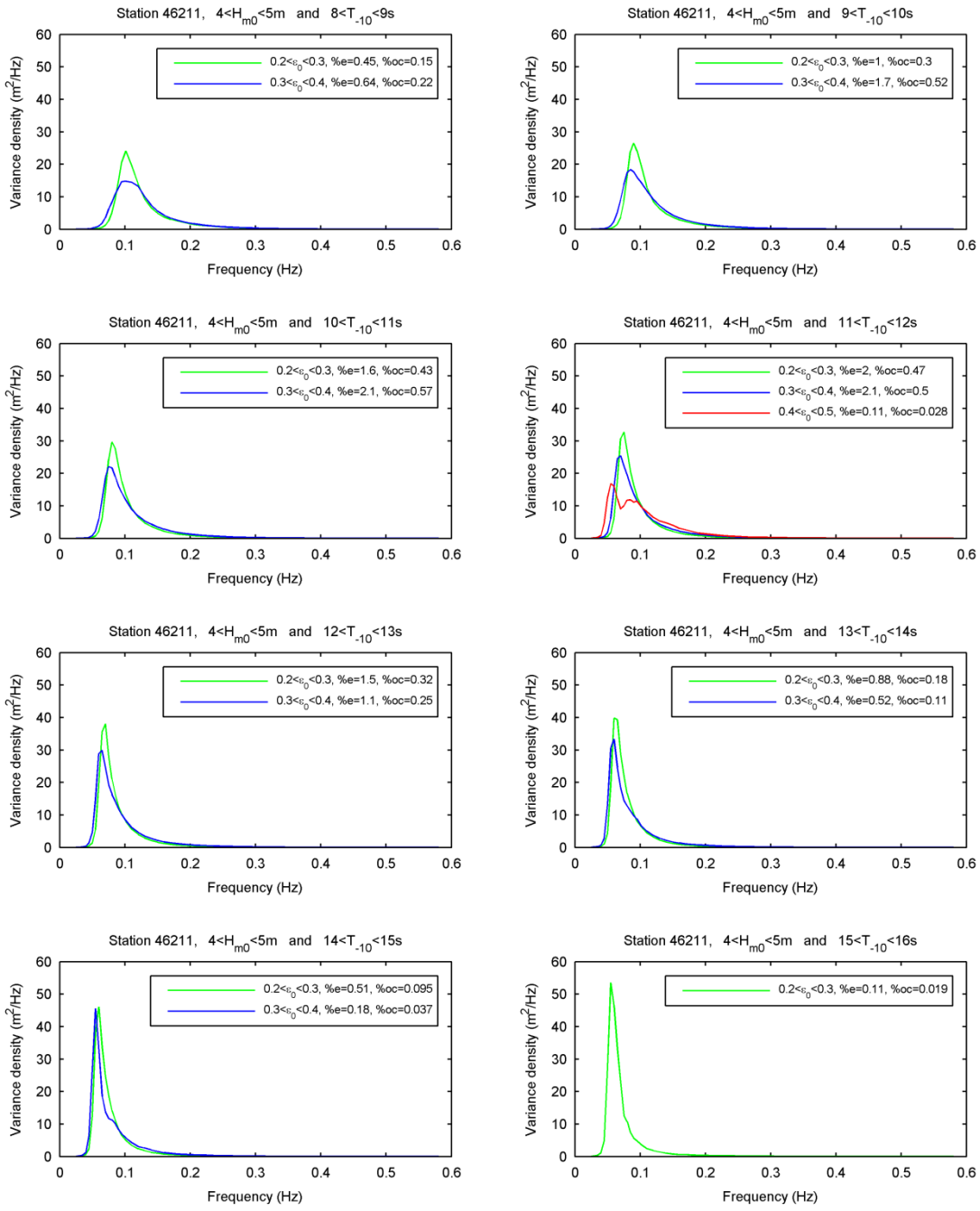

Figure A 8. Representative spectra for station 46211, 4<H_{m0}<5 m.

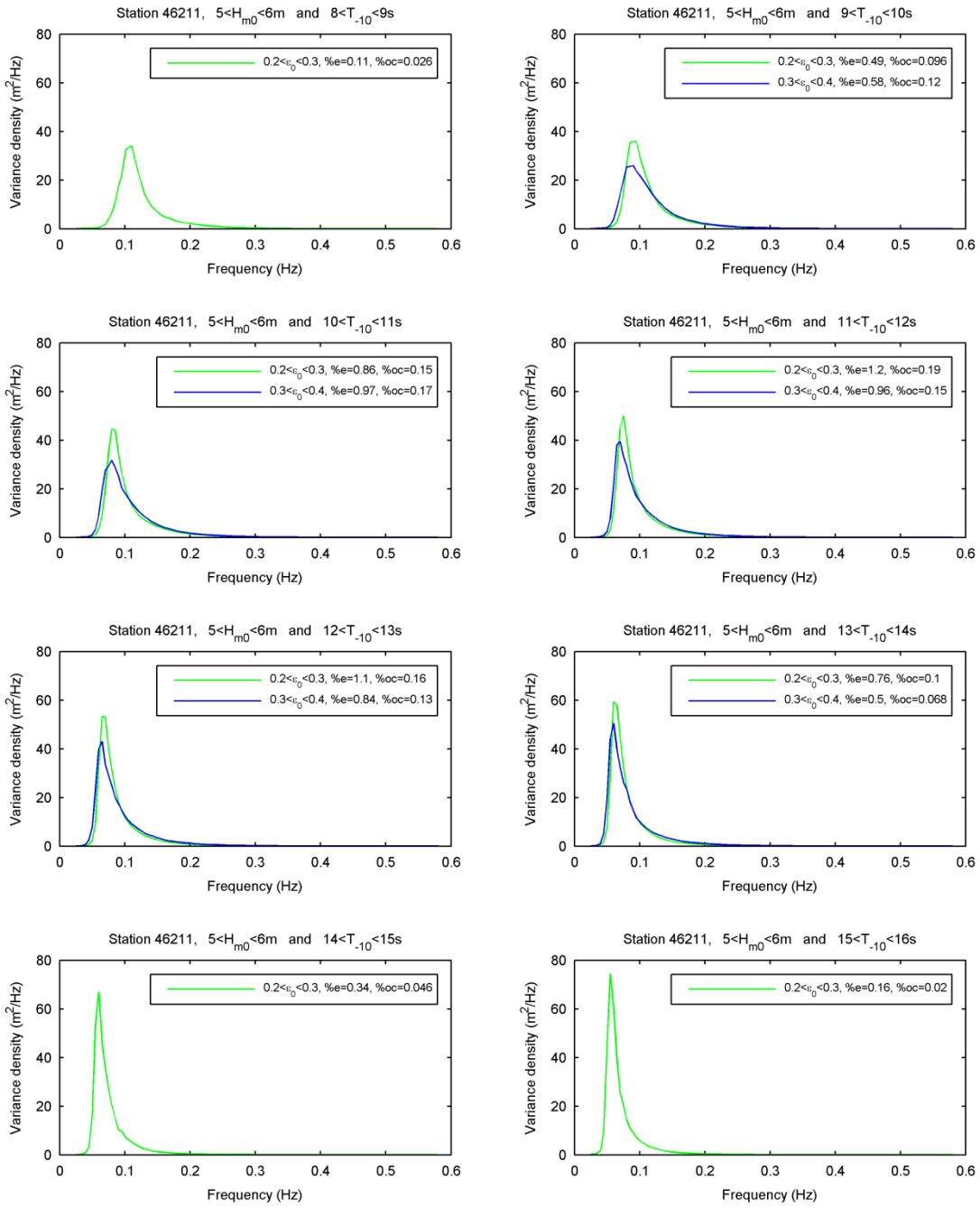

Figure A 9. Representative spectra for station 46211, 5<H_{m0}<6 m.

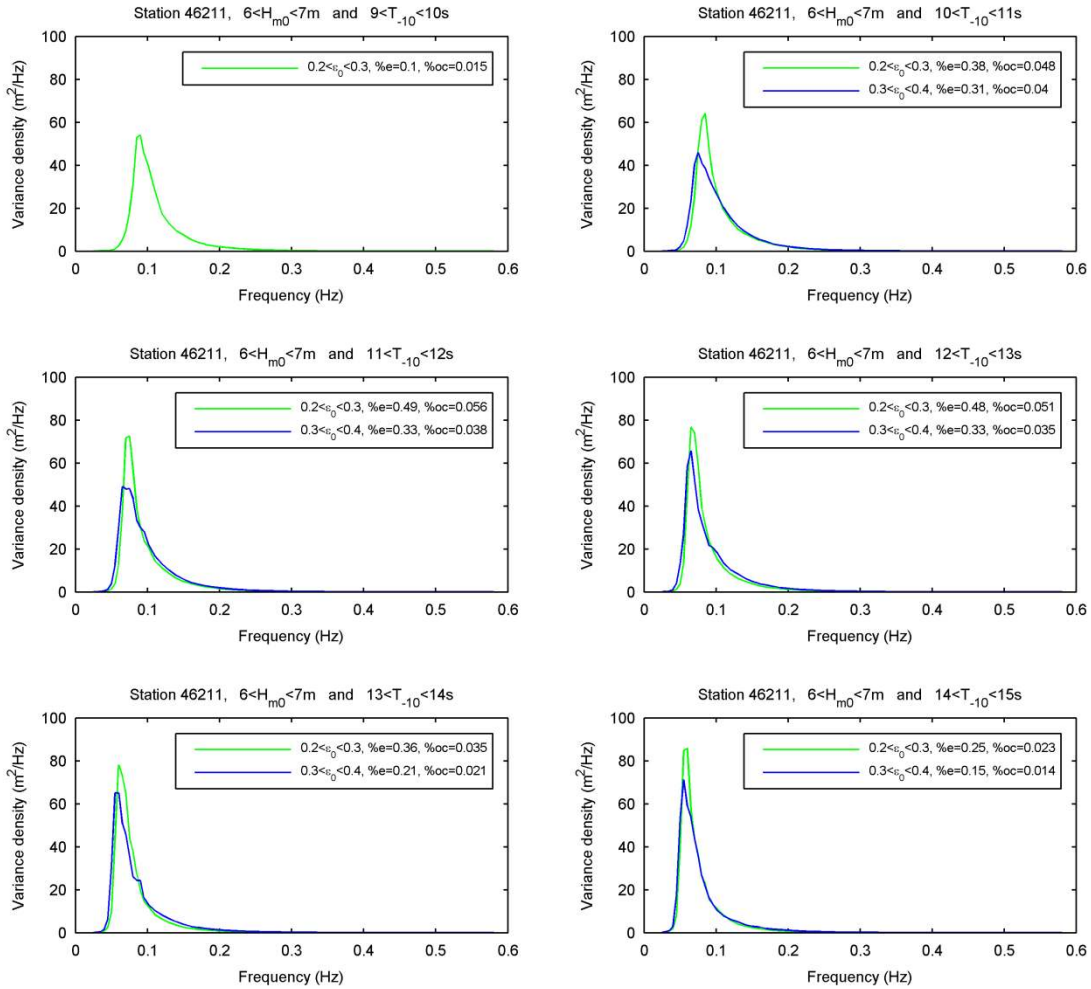

Figure A 10. Representative spectra for station 46211, 6<H_{m0}<7 m.

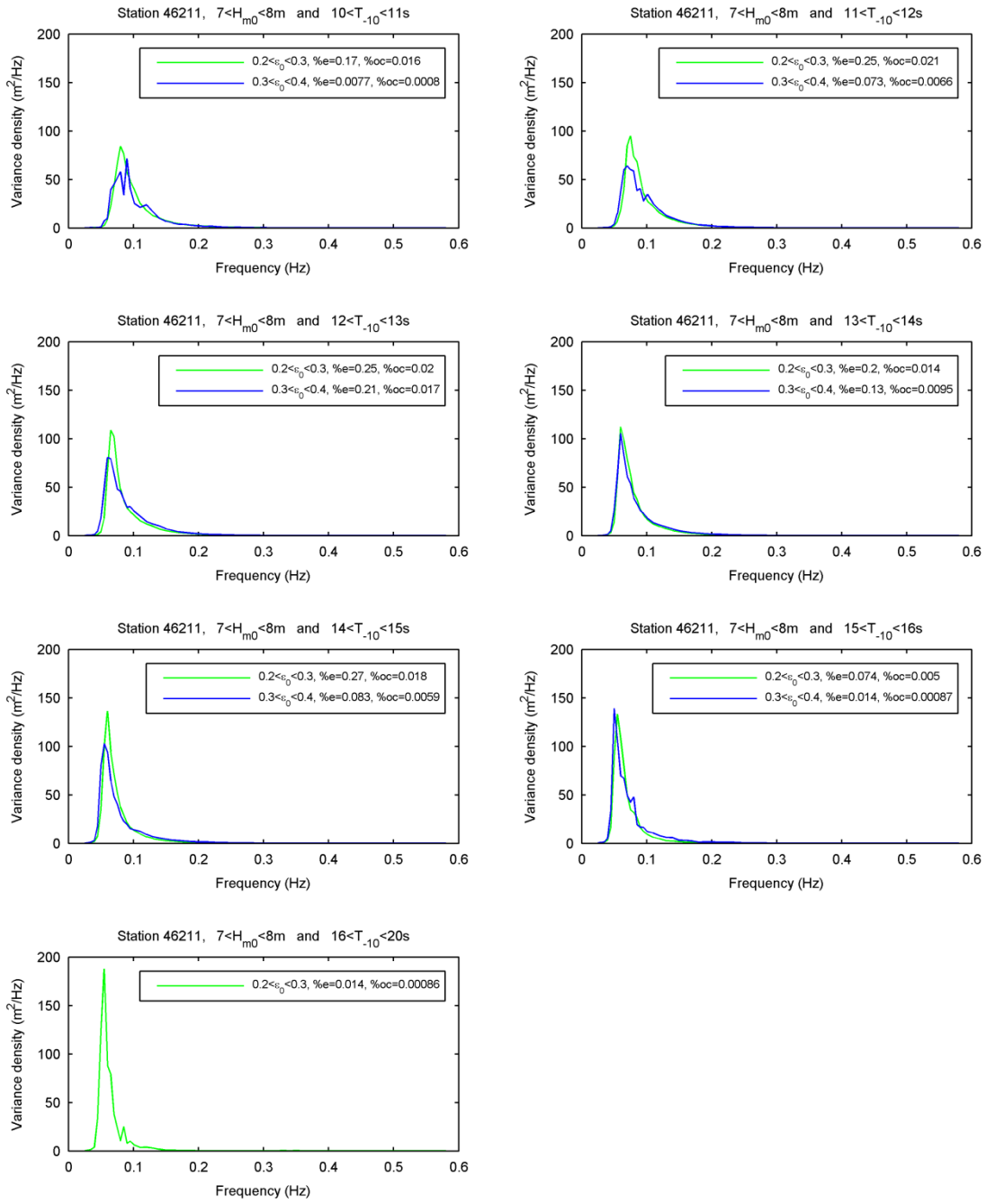

Figure A 11. Representative spectra for station 46211, 7<H_{m0}<8 m.

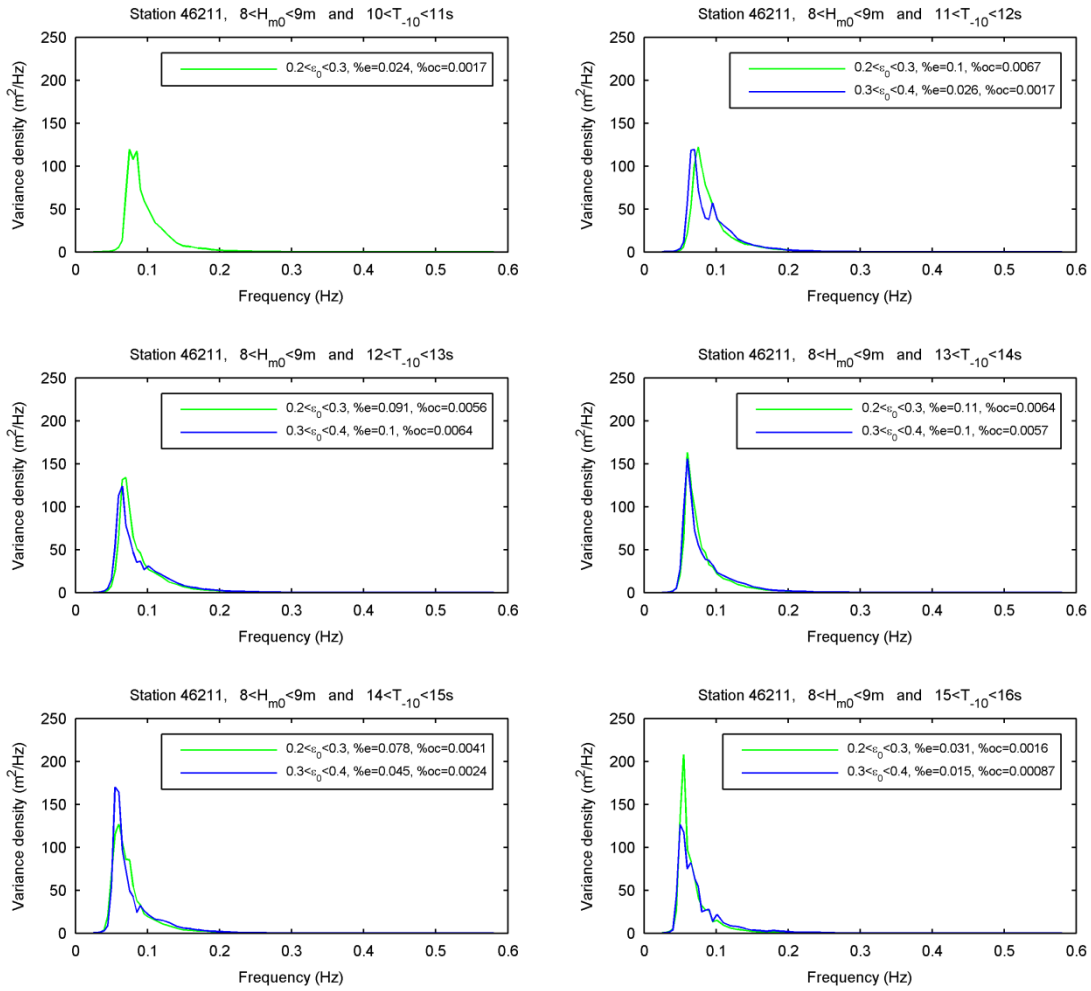

Figure A 12. Representative spectra for station 46211, 8<H_{m0}<9 m.

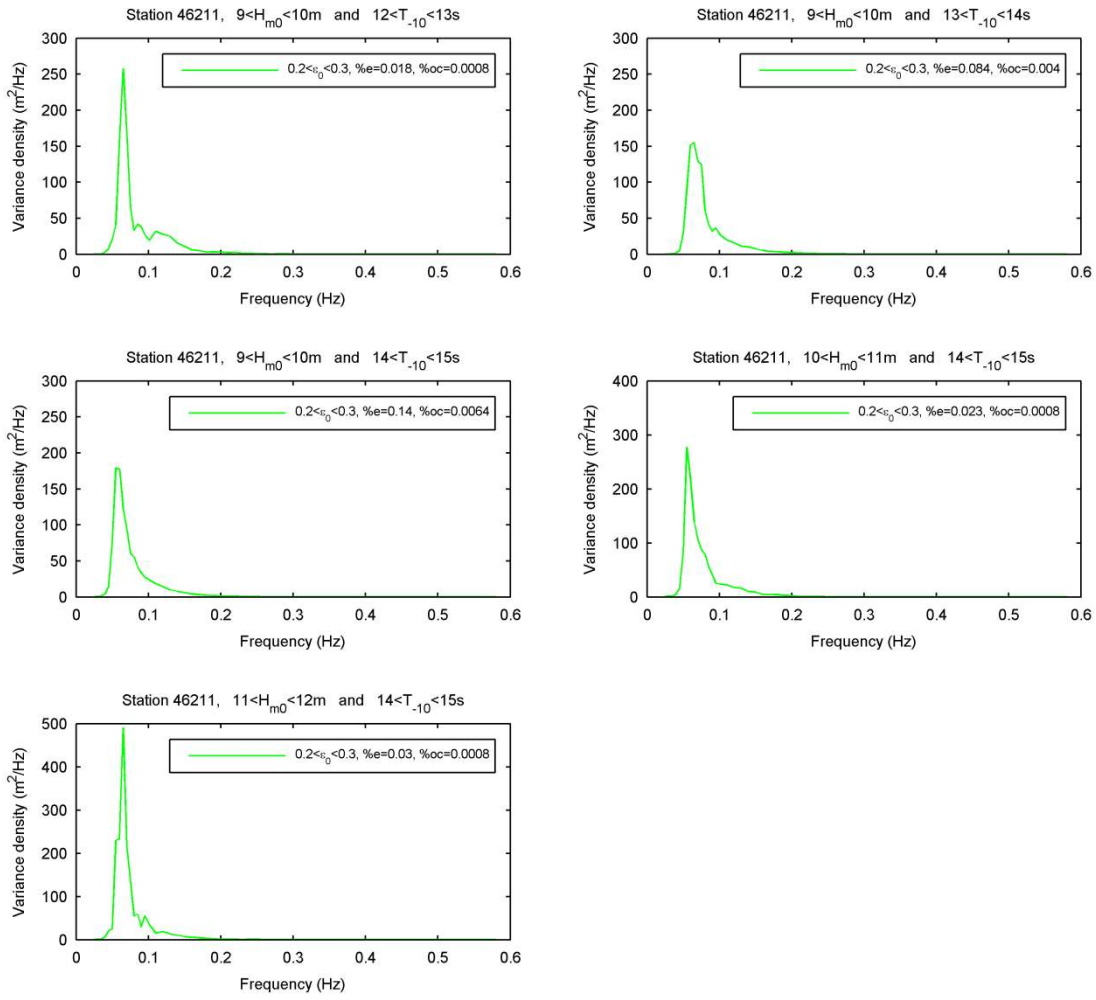

Figure A 13. Representative spectra for station 46211, H_{m0}>9 m.